Changes in Kuroshio Current dynamics and East Asian monsoon variability during the last 26 kyr

Pierrick Fenies, Maria-Angela Bassetti, Natalia Vazquez Riveiros, Christophe Menniti, Clément Frigola, Nathalie Babonneau, Gueorgui Ratzov, Shu-Kun Hsu, Chih-Chieh Su

Changes in Kuroshio Current dynamics and East Asian monsoon variability during the last 26 kyr

Pierrick Fenies[1], Maria-Angela Bassetti[1], Natalia Vazquez Riveiros[2], Christophe Menniti[1], Clément Frigola[3,4], Nathalie Babonneau[2], Gueorgui Ratzov[5], Shu-Kun Hsu[6,7], Chih-Chieh Su[8].

[1]CEFREM, Université de Perpignan Via Domitia, UMR 5110, CEDEX, 52 Avenue Paul Alduy, Perpignan, 66860, France

[2]Geo-Ocean, UMR 6538, CNRS-Ifremer-UBO-UBS, France

[3]LUSAC, Université de Caen Normandie, Cherbourg-en-Cotentin, France

[4]Conservatoire National des Arts et Métiers, INTECHMER, Cherbourg-en-Cotentin, France

[5]Université Côte d'Azur, CNRS, Observatoire de la Côte d'Azur, IRD, Géoazur, Nice, France

[6]Department of Earth Sciences, National Central University, Taoyuan, 32001, Taiwan

[7]Institute of Earth Sciences, Academia Sinica, Taipei, 11529, Taiwan

[8]National Taiwan University, Institute of Oceanography, 1, Sec. 4, Roosevelt Road, Taipei City 106, Taiwan, ROC

Pierrick Fenies: pie.fenies@gmail.com (corresponding author)

Abstract

The Kuroshio Current flows northward along the east coast of Taiwan toward the Okinawa Trough and the East China Sea, but its dynamics and trajectory were probably different during the Last Glacial Maximum (LGM) due to the globally lower sea level that could have caused a (debated) deflection of the current along the eastern edge of the Ryukyu Arc.

Core MD18-3532 has been recovered in an intra-slope basin of the Ryukyu accretionary prism, currently disconnected from the Kuroshio Current, but would have been on its trajectory in case of a NE deflection. Measurements of clay mineral assemblages and illite crystallinity revealed that Taiwan has been the main sediment source at this site over the last 26 kyr. The significantly higher sedimentation rate from the Last Glacial Maximum to the Bølling–Allerød compared with the period from the Younger Dryas to the Holocene, coupled with very low $\delta^{15}N_{sed}$ during LGM and Heinrich Stadial 1, provide evidence for the transport of sediments and *Trichodesmium* spp. cyanobacteria by the partially deflected Kuroshio Current toward the eastern edge of the Ryukyu Arc. Combined with $\delta^{13}C_{org}$, TOC, TN, and XRF analyses, an increase in primary productivity has been observed during LGM and Heinrich Stadial 1. This would have been caused by an enhanced East Asian Winter monsoon winds resulting in the deepening of the mixed layer that would have led to the upwelling of the Kuroshio Current nutrient-enriched subsurface waters to the oligotrophic surface waters, and the supply of dust-borne iron from the Chinese Loess Plateau.

Keywords

Kuroshio Current deflection; NW Philippine Sea; Taiwan paleoceanography; primary productivity; last deglaciation; *Trichodesmium* spp.

1 Introduction

The Kuroshio Current is the western boundary current of the North Pacific Subtropical Gyre. It flows northward along the eastern coast of East Asia (Fig. 1a), transferring heat, salinity and moisture from the Indo Pacific Warm Pool to the high latitudes. While its surface water is oligotrophic, marked by low concentration of chlorophyll-a (Chen et al., 2022) reflecting reduced phytoplanktonic activity, the Kuroshio Current transports large quantities of nutrients on the subsurface (300 – 600 m; maximum core of the nutrient flux at 400 – 500 m depth) (Chen et al., 2017; Guo et al., 2012). It is also at the origin of a "water barrier" effect in the East China Sea preventing the export of sediments from Chinese rivers (e.g. Yangtze River) to the Okinawa Trough during summer. This "water barrier" effect decreases during the winter, enhancing the export of sediments to the Okinawa Trough (Zheng et al., 2016).

As a result of this transfer of heat and moisture, the Kuroshio Current has a major impact on global scale by regulating the thermal balance between low and high latitudes, and on regional scale by regulating local climate and ocean dynamics (Hu et al., 2015). The gradual intensification of the Kuroshio Current over the deglaciation under the influence of East Asian Monsoon changes and the El Niño Southern Oscillation is well established (Li et al., 2020; Lim et al., 2017; Zheng et al., 2016; Zou et al., 2021). However, over the past two decades, the Kuroshio Current has been the subject of debate (Li et al., 2020; Lim et al., 2017; Ujiié and Ujiié, 1999; Vogt-Vincent and Mitarai, 2020; Wang et al., 2015; Zheng et al., 2016) regarding whether it was still able to flow through the Yonaguni Depression and remain in the Okinawa Trough, or whether it was deflected eastwards along the eastern edge of the Ryukyu Arc, as a result of the ~130 m drop in sea level (Lambeck et al., 2014) during the Last Glacial Maximum (LGM; 23.0 – 19.0 thousands of years ago; ka afterwards) (Mix et al., 2001). At

glacial/interglacial and stadial/interstadial scale, the deflection of the Kuroshio Current pathway out of the Okinawa Trough may affect East Asia and the East China Sea through changes in East Asian Summer Monsoon (EASM) rainfall patterns (Sasaki et al., 2012), the range of East Asian Winter Monsoon (EAWM) winds propagation (Pan et al., 2018), the ability of typhoons to sustain themselves with the heat and moisture of the surface ocean (Fujiwara et al., 2020; He et al., 2022; Liu and Wei, 2015; Wu et al., 2008), and through primary productivity changes outside and inside the Okinawa Trough (Chen, 2000).

Previous studies based on planktonic foraminifera (Ujiié and Ujiié, 1999; Ujiié et al., 2003), clay mineral analysis (Diekmann et al., 2008; Dou et al., 2010) and Sr-Nd isotopes (Dou et al., 2012) suggest a complete deflection of the Kuroshio Current from the Okinawa Trough toward the eastern edge of the Ryukyu Arc during LGM and its return to the Okinawa Trough since at least 14 ka. Other studies using geochemical (Lim et al., 2017; Xu et al., 2019), mineralogical (Li et al., 2019), paleotemperature proxies (Kim et al., 2015; Li et al., 2020) and modeling results (Vogt-Vincent and Mitarai, 2020; Zheng et al., 2016) suggest that the Kuroshio Current did not deflected and would have persisted, albeit weakly, in the Okinawa Trough during the low sea level period, beginning to strengthen since ~14 ka.

These previous studies are mainly based on sediments collected in the Okinawa Trough, and little attention has so far been paid to the northwestern Philippine Sea, south of the Ryukyu Arc (Fig. 1a), where deflection, if any, would have occurred. To fill this gap, in this study we analyze sediment core MD18-3532, located in an intra-slope basin of the Ryukyu accretionary prism in the northwest Philippine Sea (Fig. 1b). This core is currently disconnected from the Kuroshio Current, but might have been on its pathway during the low sea level period if it had deflected eastward.

The Kuroshio Current carries sediments delivered to the surface waters by eastern Taiwanese rivers (Diekmann et al., 2008; Dou et al., 2012; Li et al., 2019; Wang et al., 2015). A change in the amount and/or source of sediment could therefore be an indicator of the deflection of the Kuroshio Current or a weakening of its "barrier effect" that prevents the offshore export of sediments from Taiwan (Fig. 1b). Also, the emergence of the East China Sea shelf during the glacial low sea level drove the migration of the Yangtze River mouth across the shelf to the border of the Okinawa Trough, with those sediments being carried directly into the Okinawa Trough (Dou et al., 2012, 2010; Li et al., 2019) and possibly to the Ryukyu accretionary wedge area, becoming an additional sediment sources. Finally, enhanced EAWM during LGM and Heinrich Stadial 1 (HS1; 18.0 – 14.7 ka) (Denton et al., 2010) might have transported dust from Chinese Loess Plateau to the Philippine Sea as evidenced by previous studies (Jiang et al., 2016; Wan et al., 2012; Xu et al., 2015). Therefore, in order to constrain potential changes in sediment supply and sources, we have investigated the provenance of the sediments by using clay minerals and illite crystallinity as sediment source indicators (Dou et al., 2010; Li et al., 2012; Nayak et al., 2021) and sedimentation rate variability.

In addition, the Kuroshio Current is well-known to carry abundant *Trichodesmium* spp. cyanobacteria (Chen et al., 2008; Shiozaki et al., 2015), characteristic of its oligotrophic surface waters (Chen et al., 1995; Kodama et al., 2014), that generate significant nitrogen fixation compared to the rest of the Philippine Sea (Liu et al., 1996; Shiozaki et al., 2015). Therefore, we have also used sedimentary $\delta^{15}N$ ($\delta^{15}N_{sed}$) to reconstruct changes in nitrogen fixation that might indicate a deflection of the Kuroshio Current rather than a weakening of its "barrier effect".

Finally, the Kuroshio Current transports nutrients to the subsurface which when brought to the surface lead to the increase in primary productivity (Chen et al., 2022; Chen, 2000). During Marine Isotope Stage 2 (MIS 2; 27.8 – 14.7 ka; Sanchez Goñi and Harrison, 2010), the combination of a deflected Kuroshio Current with enhanced EAWM winds might have increase the primary productivity by supplying dust-borne iron to the study area and deepening the mixed layer, causing upwelling of Kuroshio Current nutrient-rich subsurface water. Therefore, using organic and inorganic geochemical proxies (TOC, TN, $\delta^{15}N_{sed}$, $\delta^{13}C_{org}$, Br/Al, Ti/Al and Fe/Al) combined with previous geochemical proxies, we investigate changes in the paleoproductivity in the northwestern Philippine Sea that might indicate the partial deflection of the Kuroshio Current.

2 General setting

Taiwan is located along the Eurasian margin (Fig. 1a), between 21°54'N and 25°18'N, and is climatically under the influence of the EASM and typhoons (Chen and Chen, 2003; Chen et al., 2010) that generate in the West Pacific Warm Pool (Gray, 1977). The hydrological regime is characterised by heavy rainfall comprised between 1500 – 2500 mm yr^{-1}, reaching 5000 mm yr^{-1} in the north and north-east of Taiwan (Li et al., 2013; Resentini et al., 2017). The large surrection rate (5 – 20 mm yr^{-1}; Ching et al., 2011; Hsu et al., 2018) is compensated by an average erosion rate of 1 to 10 mm yr^{-1} over the whole island, which can reach 30 to 60 mm yr^{-1} locally (Dadson et al., 2003). This erosion causes an important and rapid export of sediments to the ocean by hypopycnal and hyperpycnal flows (Dadson et al., 2005; Mulder et al., 2003) that reach 208 to 332 Mt yr^{-1}, including 68.5 (± 35.4) (±2σ; as all the ±SD hereafter) Mt yr^{-1} through the north-eastern rivers of Taiwan (Lanyang – Hualian rivers) (Resentini et al., 2017). This results in high sedimentation rates in the coastal regions of Taiwan of few hundred

cm kyr^{-1} (see supplementary materials) (Li et al., 2009; Wei et al., 2005; Yu et al., 2017). High sedimentation rates are also observed in the western mud area of the East China Sea shelf (100 – 300 cm kyr^{-1}) related to the transport of sediments from the Yangtze River (480 Mt yr^{-1} ; Xu et al., 2007) and, to a lesser extent, transport of the Taiwanese rivers (Dong et al., 2020).

North East Taiwan, in the region of the Ryukyu accretionary prism, hyperpycnal flows pass through the Hoping Canyon to the Nanao Basin (Fig. 1b) (3700 m below sea level or b.s.l.). These flows possibly do not cross the submarine morphological barrier of the Nanao Rise (3 400 m b.s.l.). The absence of pyrrhotite, a characteristic mineral of the Central Range (Horng et al., 2012), in the sediments of the East Nanao Basin (Hsiung et al., 2017), supports this assumption. Moreover, a reduced occurrence of turbidites in the East Nanao Basin (4 600 m b.s.l.) compared to the Nanao Basin has been observed (Nayak et al., 2021). Generally speaking, the finest sediment fraction of turbidity flows may remain in suspension and cross over topographical ridges of hundreds of meters (Kneller and Buckee, 2000). However, the Yaeyama Ridge (2 800 m b.s.l.), a barrier separating the East Nanao Basin and the MD18-3532 basin, is about 1 800 m high (Fig. S1 in Supplementary Material), too high for allowing the totality of the turbidity flows to cross the obstacle, that could be partial at the most and transporting only the finest silts, isolating the intra-slope basins from sedimentary inputs from Taiwan and the Ryukyu Arc (Fig. 1b) (Hsiung et al., 2017). The sediments constituting the hypopycnal flows are diverted to the Okinawa Trough by the Kuroshio Current (Fig. 1a).

The Kuroshio Current emerges from the bifurcation of the North Equatorial Current, between 8 and 17°N (Qiu et al., 2015) and flows northward along Philippines and Taiwan eastern coasts before entering the Okinawa Trough in the East China Sea through the Yonaguni Depression (sill depth ±775 m) (Qiu, 2001) and the Kerama Gap (sill depth ±1100 m)

159 (Na et al., 2014). It exits the East China Sea through the Tokara Strait (sill depth ±690 m) (Qiu,
160 2001) and joins the North Pacific (Fig. 1a). Nowadays, east of Taiwan, the Kuroshio Current
161 transports a volume of 11 – 23 Sv (1 Sv = 10^6 m^3 s^{-1}) for a maximum current velocity between
162 0.7 and 1.4 m s^{-1} (Jan et al., 2015). Its boundary can be delimited by the 0.2 m s^{-1} marine
163 isotach at 30 m depth based on historical ADCP data set (Jan et al., 2015). Within these limits,
164 its width is between 85 and 135 km for a thickness of 400 to 600 m, centred at 122°E (Jan et
165 al., 2015).

166 Below 600 m, the intermediate waters flow northwards but at a speed of less than 0.2 m
167 s^{-1}. When they reach the Ilan Ridge, which bridges Taiwan and the Ryukyu Arc and constitutes
168 the bottom of the Yonaguni Depression, the intermediate waters are deflected eastward,
169 along the eastern edge of the Ryukyu Island, forming the Ryukyu Current (Wang et al., 2019)
170 (Fig. 1a). It exhibits a main core with a velocity maximum of 0.2 to 0.1 m s^{-1} between 600 and
171 1000 m depth (Wang et al., 2019). East of the Kuroshio Current, the velocity of the Ryukyu
172 Current is not enough to drag waters above its main core (Wang et al., 2019). However, the
173 Ryukyu Current intensifies along the its path, and south of Okinawa, is strong enough to
174 extend its influence to the surface and drag water with it (Wang et al., 2019).

175 As a geostrophic current belonging to the North Pacific subtropical gyre, the Kuroshio
176 Current intensity is associated with the horizontal gradient of wind stress on the ocean surface
177 (Hu et al., 2015). Thus, easterlies and westerlies apply respectively a negative and positive
178 wind stress curl over the equatorial Pacific; when negative, it causes an equatorward
179 migration of the North Equatorial Current compensated by the intensification of the poleward
180 Kuroshio Current transport to conserve mass balance, and conversely when positive (Hu et al.,
181 2015; Qiu and Lukas, 1996). This wind stress curl is strongly influenced by the East Asian

Monsoon and the El Niño Southern Oscillation. During EASM and La Niña phase, strengthened easterlies induce an increase of the negative wind stress curl, leading to a equatorward migration of the bifurcation and hence an intensification of the Kuroshio Current. Conversely, during EAWM and El Niño phase, the strengthened westerlies and weakened easterlies generate a positive wind stress curl, leading the poleward migration of the bifurcation and hence a weakening of the Kuroshio Current (Hu et al., 2015; Qiu and Lukas, 1996).

3 Materials and methods

The 23 m piston core MD18-3532 (23°28.88'N, 123°5.89'E; water depth: 4325 m) was recovered during the EAGER Cruise of the R/V Marion-Dufresne II in 2018. It was collected at 150 km off the coast of Taiwan, in an intra-slope basin of the Ryukyu arc accretionary wedge and out of the present-day mainstream of the Kuroshio Current (Fig. 1a). It is composed of dark grey clay with no evidence of turbiditic sediment sequences or large mass transported deposits, neither at the naked eye lithology observation, nor on general geometry on seismic profiles (N. Babonneau and G. Ratzov, unpublished data). Few millimetre-thick silt/fine sand layers concentrated in the uppermost 3 m of the core are found, related to the deposition of the queue of fine-grained turbidites derived from turbidite flows thick enough to surmount the topographic barrier and reach East Nanao Basin. Volcanic glass has been observed under binocular microscope in the > 150 µm size fraction at 165.5 cm depth. No tephra layers can be found at the naked eye inspection.

The age model was built using 13 radiocarbon dates (Table 1) on mixed planktonic foraminifera measured at Alfred-Wegener Institute (Bremerhaven, Germany), using a MICADAS-Accelerator Mass Spectrometry (AMS) and at Laboratoire des Sciences du Climat et de l'Environnement (Saclay, France) using the ECHoMICADAS-AMS facilities. They were

converted to calendar ages using Oxcal software version 4.4.4 (Ramsey, 2008) and the Marine20 calibration curve (Heaton et al., 2020). A local correction of the reservoir age of 86 (±40) years was applied (Dezileau et al., 2016). The volcanic glass shards at 165.5 cm corresponding to the 7 300-year-old Kikai-Akahoya (K-Ah) eruption (Matsu'ura et al., 2021) confirms the age model (Fig. 2).

The sediment core was scanned at 1 cm resolution using an AVAATECH XRF core scanner at IFREMER laboratory "Geo-Ocean" (Plouzané, France) to determine the semi-quantitative elemental composition of the sediment in counts per second (Richter et al., 2006). The ln(Br/Al) ratio is commonly used to qualitatively reconstruct the relative abundance of marine organic matter and to differentiate it from terrestrial organic matter, since Br is particularly abundant in the marine realm due to the synthesis of organic bromine-laden compounds by bacteria and microalgae (Channell et al., 2019; Harvey, 1980; Hillenbrand et al., 2021; Mayer et al., 2007; Nieto-Moreno et al., 2011; Ziegler et al., 2008). Ln(Ti/Al) and ln(Fe/Al) can be used to identify the contribution of secondary terrestrial sources of sediments by highlighting their difference in composition of terrigenous elements with the main source, such as aeolian dust supplies in an environment dominated by fluvial inputs (Calvert and Pedersen, 2007; Croudace and Rothwell, 2015; Govin et al., 2012; Martinez-Ruiz et al., 2015). The XRF ratios were smoothed by a 30-point moving average using XLSTAT software (Addinsoft, 2016).

One-cm thick samples were retrieved from the core approximately every 10 centimetres (n = 264), corresponding to an average resolution of 100 years. Three-gr subsamples were used for geochemical analysis and the rest was sieved at 63 µm to separate the silt-clay from the sand fraction. Carbon and nitrogen isotopic ($\delta^{15}N_{sed}$, $\delta 13C_{org}$) analyses, as well as measurements of total carbon (TC), total nitrogen (TN) and total organic carbon (TOC) were

carried out on those samples. $\delta^{15}N_{sed}$, $\delta^{13}C_{org}$, TC and TN were analysed on freeze-dried, grounded, and weighed samples at CEFREM laboratory (University of Perpignan, France). $\delta^{15}N_{sed}$, $\delta^{13}C_{org}$ subsamples were decarbonated using repeated additions of 2 $mol.L^{-1}$ of concentrated hydrochloric acid (HCL) until no effervescence was observed. Isotopic values were measured with a Eurovector 3000 elemental analyser coupled to a GVI-Isoprime mass spectrometer (EA-IRMS). Values are expressed in per mil (‰) relative to the Vienna Pee Dee Belemnite standard (V-PDB) for $\delta^{13}C_{org}$ and AIR for $\delta^{15}N_{sed}$. All samples were measured at least in duplicate at CEFREM laboratory (University of Perpignan, France). For each series of measurements, High Organic (HO) sediment B2151 and Low Organic (LO) sediment B2153 certified standards were analyzed at the beginning and end of the series. Standard values and errors, as well as the analytical precision and accuracy are reported in Table S1.

TC and TN values were measured on a CHN Elementar at CEFREM laboratory (University of Perpignan, France) and values are expressed in percentage of dry weight (%). TOC was calculated by dividing (i) the mass of absolute C by (ii) the total mass of the sample multiplied by 100. TOC and TN can originate from primary productivity and/or continental input (Hilton et al., 2010; Kao et al., 2014), and they are often used to reconstruct changes in primary productivity (Meyers, 1997; Stein, 1991). Here, TOC has been compared to Br/Al to distinguish marine organic matter from terrestrial input, and a marine vs. continental $\delta^{13}C_{org}$ mixing model has been performed in order to estimate the terrestrial contribution (F_{terr} $\delta^{13}C_{org}$) to the organic C accumulation and $\delta^{13}C_{org}$ signature. The equation used take the form : $Fterr = (X - X_M) / (X_T - X_M)$, with X the $\delta^{13}C_{org}$ of the sample, X_M the marine $\delta^{13}C_{org}$ end-member and X_T the terrestrial $\delta^{13}C_{org}$ end-member (Kandasamy et al., 2018). For this purpose, the $\delta^{13}C_{org}$ terrestrial end-member has been estimated at -22.8‰ and the marine end-member at -20.0‰ (Goericke and Fry, 1994; Kao et al., 2003).

The clay minerals were analysed using the XRD PANalytical X'Pert PRO at the Centre Européen de Recherches Préhistoriques (Tautavel, France). The analyses were conducted on the 2 µm fraction of 65 evenly distributed samples after decarbonation and oxygenated water degradation of organic matter. The identification and semi-quantification of the different clays was done based on the position and intensity of peaks. Illite and chlorite were analysed based on their main peaks at 14 and 10 Å respectively. Kaolinite was measured based on the ratio between the intensity of the shoulder at 3.5 Å and the intensity of the (002) chlorite peak at 5 Å. The percentages of each clay mineral were determined with respect to the abundance of all detected minerals including clay, quartz, and feldspars peaks at 4.26 and, 3.24-3.18 Å respectively. Illite crystallinity has been calculated as the full width at half maximum of the main illite peak. It can be used to determine the degree of chemical (high values) or physical (low values) alteration of a rock (Li et al., 2012) or as an index of provenance in the case where the source is partly composed of metamorphic rocks (Jaboyedoff et al., 2001; Verdel et al., 2012).

4 Results

4.1 Age model and sedimentation rate

The age model indicates that the core MD18-3532 covers the last 26 kyr (Fig. 2, Table 1). Significant variations in sedimentation rate can be observed and coincide with the depths at which radiocarbon measurements were measured, indicating they are artefacts generated by the calculation model that has been run using only the dated points (Fig. 2). Two periods can be nonetheless highlighted: a “high” sedimentation rate period of 177 cm kyr^{-1} from 13.3 (±0.5) to 24.8 (±0.6) ka, and a “low” sedimentation rate period of 38 cm kyr^{-1} from 3.5 (±0.3) to 13.3 (±2.5) ka (Fig. 2 and 3a). Although the exact timing of the transition, 13.3 ±2.5 (0.5) ka

toward the younger (older) date, has a large error, the transition between these two periods takes place during BA.

4.2 Illite crystallinity, clay minerals abundance and grain size

The clay minerals are composed of illite, chlorite and kaolinite (Table 2) and variations are not substantial throughout the core, although higher percentages of illite and chlorite are observed in the Holocene (11.7 – 0.0 ka) (Walker et al., 2009) compared to MIS 2, due to the decrease in kaolinite (Fig. 3b). Same as clay minerals, illite crystallinity remain relatively constant throughout the core (Table 2; Fig. 3c). The weight percentage of the < 63µm fraction ranges from 81.0 to 99.9 with an average of 99.0 (±4.0) and, despite some fluctuations, remains stable throughout the core (Fig. 3d).

4.3 X-ray fluorescence (XRF)

Ln(Br/Al) values range from -3.70 to -0.46 with an average of -2.67 (±0.72), Ln(Fe/Al) range from 2.87 to 4.31 with an average of 3.27 (±0.34) and Ln(Ti/Al) range from 0.61 to 1.48 with an average of 0.88 (±0.25) (Fig. 3e). These three XRF ratios show a similar trend with a gradual increase during the pre-LGM and LGM with a maximum reached during the Late Glacial (LG; 19.0 – 18.0 ka) and HS1, before beginning to decrease at the end of HS1, from 16 to 7 ka. After 7 ka, the three ratio start to rise again (Fig. 3e). A similar evolution of the trend can also be stated by Spearman correlation. Both terrigenous ln(Fe/Al, Ti/Al) ratios show a very strong correlation with each other ($r = 0.91$, p-value < 0.001) and a moderate correlation rate with ln(Br/Al) ($r = 0.64 – 0.65$, p-value < 0.001) (Table S2). The Spearman correlation coefficient with ln(Br/Al) increase after smoothing the data using a 30-order moving average ($r = 0.74$, p-value < 0.001) (Table S3).

4.4 Isotopic geochemistry

$\delta^{15}N_{sed}$ values range from -1.6 to 7.4‰ with an average of 3.1‰ (±3.2) (Fig. 3f). They show relatively high values during the pre-LGM before abruptly decreasing at the beginning of LGM. Then, they observe a sharp decrease to much lower values until the mid-BA, with mean values from LGM to 13.6 ka. After the mid-BA, the $\delta^{15}N_{sed}$ rises steeply and stabilize on a plateau from Younger Dryas (12.9 – 11.7 ka) (Clark et al., 2012) until the Holocene (Fig. 3f).

$\delta^{13}C_{org}$ values range from -22.5 to -19.0‰ with an average of -21.3‰ (±1.1) (Fig. 3g). The record shows high values during the pre-LGM then a decrease during LGM, before starting to increase again during LG to reach a maximum during mid-HS1, around 17.5 – 16 ka. From 16 ka, $\delta^{13}C_{org}$ values start to decrease progressively to reach a minimum plateau after 8 ka (Fig. 3g). The marine vs. continental $\delta^{13}C_{org}$ mixing model values show that the contribution of marine organic carbon is highest during HS1 and pre-LGM. They show a more moderate marine contribution during LGM, LG and BA, and an increase of the terrestrial contribution since the end of HS1 to a maximum during the Holocene (Fig. 3h).

4.5 Organic geochemistry

TOC values range from 0.33 to 0.79% with an average of 0.57% (± 0.17) (Fig. 3i). They show an increase from the pre-LGM to HS1, then a decrease from Bølling–Allerød (BA; 14.7 – 12.9) (Clark et al., 2012) until reaching a minimum during the Holocene (Fig. 3i). TN values range from 0.05 to 0.14% with an average of 0.09% (±0.03) (Fig. 3j). They show an increase from the pre-LGM to LG, then a decrease until the mid-BA, before rising slightly during the Holocene (Fig. 3j).

5 Discussion

5.1 Origin of sediments in core MD18-3532

Clay minerals relative abundance show that the sediments of core MD18-3532 are dominated by illite and chlorite with traces of kaolinites (Fig. 4e). In the South and East China Seas, clay mineral assemblages are commonly used to reconstruct the source of terrigenous sediments (Diekmann et al., 2008; Dou et al., 2010; Liu et al., 2016, 2010; Steinke et al., 2008; Wan et al., 2010). Previous studies have evidenced that in the region, three sources are characterized by dominance of illite and chlorite with rare presence of kaolinite: (i) the Yangtze River and the East China Sea shelf, (ii) the Taiwan island and (iii) the Chinese Loess Plateau (Diekmann et al., 2008; M. He et al., 2013; Li et al., 2012; Nayak et al., 2021; Wan et al., 2007; Zhao et al., 2017).

In Taiwan island, the dominance of illite and chlorite is related to intense physical erosion and the rapid transfer of eroded sediments to the ocean, which prevents the chemical erosion necessary for the formation of kaolinite (Chamley, 1989; Li et al., 2012). In addition, the Central Taiwan Range is composed of polymetamorphic rocks with an abundance of slates and schists that generate illite and chlorite (Ho, 1986; Li et al., 2012; Nayak et al., 2022). Thus, kaolinite is only a minor mineral of Taiwan, mainly found in Hengchun Peninsula and Kenting Plateau, the southern tip of the Taiwan Central Range and its southern submarine plateau, and Tainan Shelf, on the SW coast, with an average concentration of 10% (Nayak et al., 2021).

The Yangtze River originates in the eastern part of the Tibetan plateau, whose high elevation (>6000 m) leads to increased erosion and cold climate, resulting in a significant formation of illite. The bedrock in the upper Yangtze watershed includes intermediate-acid igneous rocks and basic basalts which favor the formation of illite and chlorite (M. He et al.,

2013). In contrast, indexes of chemical alteration, erosion and crystallinity of illite indicate an increase of chemical weathering in the middle and downstream sections of the watershed relative to upstream (M. He et al., 2013). It is marked by an enrichment of kaolinite due to the chemical erosion of granites containing potassium feldspars and muscovite which are sources of kaolinite under chemical weathering conditions (M. He et al., 2013). Thus, Yangtze transported particulate matter deposits mostly illite and chlorite on the East China Sea shelf, with kaolinite present up to 10% on average (M. He et al., 2013; Liu et al., 2006).

The Chinese Loess Plateau clay mineral assemblage is dominated by illite and chlorite with little amount of kaolinite (6 – 10%) (Wan et al., 2007; Zhao et al., 2017). Illite and chlorite originate from the erosion of very low- to low-grade metamorphic rocks eroded by EAWM winds from northern region of the Tibetan Plateau (Ji et al., 1999), while the prevailing aridity and low temperatures in the loess region, particularly during glacial periods, limit the chemical weathering that would lead to kaolinite formation (Chamley, 1989; Maher, 2016).

Core MD18-3532 clay minerals abundance could therefore potentially be related to (i) erosion of Taiwan massifs, (ii) sediment transport from the Yangtze River, especially during low sea level periods, and (iii) airborne transport of loess sediments mainly during glacial periods. The Yangtze River source (ii) might be particularly important if we consider a weakening of the Kuroshio Current through the Okinawa Trough, and the potential establishment of a counter-current in the Okinawa Trough similar to the modern Zhejiang-Fujian Coastal Current. This latter can originated by an enhanced EAWM, transporting sediments southward. The Yangtze River contribution to the sedimentation of the southern Okinawa Trough during the deglaciation is supported by the mineralogical composition of sediment at the ODP 1202B site (Diekmann et al., 2008) (Fig. 1a). The third source would have

been particularly intense during LGM and HS1 due to intensified EAWM (E. Huang et al., 2011; Sun et al., 2012; Yang et al., 2020). It was caused by the increase of the zonal land-sea thermal contrast between Eurasia and North Pacific by the cooling of the North Hemisphere, resulting in the intensification of the Siberian High over Eurasia (Kutzbach, 1993; Sun et al., 2012) and Aleutian Low over the western North Pacific (McGee et al., 2018; Yanase and Abe-Ouchi, 2007). During HS1, the Atlantic Meridional Overturning Circulation weakening in the North Atlantic, combined with the setting of El Niño-like state in the equatorial Pacific (Clement et al., 1999; Merkel et al., 2010; Timmermann et al., 2007), would have resulted in an even stronger intensification of EAWM than during LGM as evidenced by the maximum observed in the Gulang Loess mean grain size (Fig. 4b) (E. Huang et al., 2011; Sun et al., 2012; Yang et al., 2020).

In order to disentangle the potential sediment sources we compared measured illite crystallinity values from core MD18-3532 with those measured in previous studies in sediments from Taiwan rivers, Chinese Loess Plateau, the Yangtze River and the East China Sea shelf. Illite crystallinity measured present much lower values than those of loess (C. Huang et al., 2011; Ji et al., 1999), East China Sea shelf and the Yangtze River (M. He et al., 2013) (Fig. 5). These values are characteristic of Fe-Mg rich un-weathered illite and of physically eroded greenschists typical of the Central Range of Taiwan (Li et al., 2012; Nayak et al., 2021) and the stability of these values over the past 26 kyr suggest a steady sediment source (Fig. 4f). The source of the kaolinite is more difficult to ascertain, but given the clearly Taiwanese signal of illite crystallinity, we suggest that the kaolinite originates from the Hengshun Peninsula, southern Taiwan, and remobilization of Kenting Plateau sediments by erosion caused by the Kuroshio Current (Das et al., 2021).

387 However, although Taiwan appears to be the main and constant source of sediment,
388 secondary sources bringing insufficient amounts of sediment to influence the clay assemblage
389 may exist. Using ln(Fe/Al) and ln(Ti/Al), we observed an increase in these elemental ratios
390 from LGM to HS1 before starting to decrease during BA that might indicate supply of
391 terrigenous material from another source than Taiwan (Fig. 4g). As ln(Ti/Al) and ln(Fe/Al) show
392 a very strong Spearman correlation degree (r = 0.91 ; Table S2), it suggests that ln(Fe/Al) is not
393 affected by redox mechanisms and that both ratios reflect terrestrial inputs (Croudace and
394 Rothwell, 2015). Changes in these elemental ratios might be related to grain size sorting due
395 to the presence of Ti- and Fe-bearing heavy minerals in the coarse fraction (Croudace and
396 Rothwell, 2015; Zhao et al., 2011), but low abundance and small variation in the sandy fraction
397 suggest that grain size doesn't have any effect on these elemental ratios (Fig. 3d). The ln(Ti/Al)
398 and ln(Fe/Al) trends are more similar to the evolution of the EAWM winds intensity as
399 registered in the Gulang Loess mean grain size (Sun et al., 2012) and dust mass accumulation
400 rate in core MD06-3047, collected east off Philippines (Xu et al., 2015) than to sea level
401 changes (Lambeck et al., 2014) (Fig. 4b). This suggests dust-borne Fe and Ti inputs by enhanced
402 EAWM rather than related to the emergence of the East China Sea shelf and southeastward
403 migration of the Yangtze River mouth.

404 ## 5.2 Changes in the Kuroshio Current pathway

405 Given that Taiwan has been established as the major and constant source of sediment, we
406 investigate hypotheses that could explain the high sedimentation rate observed from LGM to
407 BA (Fig. 4d). From the LGM to HS1, the weakening of the easterly trade winds due to an
408 enhanced EAWM (Cheng et al., 2016; Steinke et al., 2010; Sun et al., 2012), El Niño-like
409 conditions (Clement et al., 1999b; Ford et al., 2015; Koutavas et al., 2002; Yamamoto, 2009)
410 and weakened Walker Circulation (Hollstein et al., 2018; Tian and Jiang, 2020) led to the

411 decrease of the positive wind stress curl over the equatorial North Pacific (Hu et al., 2015).
412 This would have caused the northward migration of the North Equatorial Current bifurcation
413 resulting in the weakening of the Kuroshio Current (Hu et al., 2015; Qu and Lukas, 2003; Zou
414 et al., 2021). Therefore, Kuroshio Current's decline could have caused a reduction of the
415 "barrier effect", allowing surface sediment plumes to spread eastwards, toward the study
416 area.

417 On the other hand, at least partial deflection of the Kuroshio Current along the eastern
418 edge of the Ryukyu Arc might also have transported eroded sediments from Taiwan to the
419 study site. This deflection could have been caused by the ~130 m drop in sea level during the
420 LGM (Lambeck et al., 2014) decreasing the water depth in the Yonaguni depression. This
421 would have caused an increase in the intermediate water volume diverted eastwards,
422 strengthening the Ryukyu Current and ultimately dragging the surface water to form an
423 eastern branch of the Kuroshio Current (Fig. 6).

424 Both hypotheses are consistent with an increase in the sedimentation rate from LGM to
425 BA (Fig. 4d). Previous publications observed an intensification of the Kuroshio Current in the
426 Okinawa Trough during BA (Li et al., 2020, 2019; Lim et al., 2017) (Fig. 7d and 7e) that could
427 have been induce by a renewed efficiency of the "water barrier" effect. On the other hand,
428 the sea level rise from – 100 to – 60 m during BA (Lambeck et al., 2014) (Fig. 7c) might be at
429 the origin of a decrease in the Ryukyu Current intensity by reducing the intermediate water
430 volume diverted eastward and increasing it in the Yonaguni Depression. This would have
431 resulted in the collapse of the Kuroshio Current eastern branch and intensification of the
432 Kuroshio Current in the Okinawa Trough as observed in the increase of sea surface
433 temperatures (Li et al., 2020; Sun et al., 2005) (Fig. 7d), deepening of the thermocline (Li et

al., 2020) (Fig. 7e) and in the relative contribution of detrital ferrimagnetic minerals to bulk magnetic properties (Li et al., 2019).

From 22.5 – 13.6 ka, the high sedimentation rate is concomitant with $\delta^{15}N_{sed}$ values averaging 2.1‰ (±1.3) (Fig. 7g). Those low values might be attributed to three mechanisms: (i) grain size sorting effect (Robinson et al., 2012; Schubert and Calvert, 2001), (ii) continental influence due to the main dominance of illite in Taiwanese clay mineral assemblages (Robinson et al., 2012) or (iii) nitrogen fixation by cyanobacteria (Galbraith et al., 2008; Kim et al., 2017). The high abundance and the small variation of the < 63 µm fraction (Fig. 3d) suggest that grain size sorting (i) does not have any effect on $\delta^{15}N_{sed}$ signature. The continental influence (ii) is potentially possible, as it is linked to the presence of NH_4^+ in the interfoliar space of illite clay. However, $\delta^{15}N_{sed}$ and TN data show a non-significant Spearman correlation with illite ($p > 0.05$; Table S4), indicating that illite inputs have no influence on $\delta^{15}N_{sed}$ or TN values. Furthermore, measurements in rocks from Taiwan show higher $\delta^{15}N$ values (>3‰) (Owen, 2013; Yui et al., 2009) suggesting that terrestrial input from Taiwan do not influence $\delta^{15}N_{sed}$.

Thus, we suggest that the $\delta^{15}N_{sed}$ records is mainly controlled by nitrogen fixation. The Kuroshio Current carries abundant *Trichodesmium* spp. cyanobacteria that originate in blooms around the Pacific island along its path (Chen et al., 2008; Shiozaki et al., 2015; Wu et al., 2018). Their abundance decreases with distance from the coast in east Taiwan (Chen et al., 2018) and they generate significant nitrogen fixation in the Kuroshio Current compared to the rest of the Philippine Sea (Liu et al., 1996; Shiozaki et al., 2015) with a specific $\delta^{15}N$ signature around − 0.9 ±1.0‰ (Eberl and Carpenter, 2007; Liu et al., 1996; Wada and Hattori, 1976). The observed decrease in $\delta^{15}N_{sed}$ during the period of high sedimentation rate (Fig. 7g) might have

been caused by the supply of these cyanobacteria over the study area by an eastern branch of the Kuroshio Current, suggesting rather a partial deflection of the Kuroshio Current than a decrease of the "water barrier" effect (Fig. 6). During and after BA, the collapse of the Kuroshio Current eastern branch due to the rise of sea level and the intensification of the Kuroshio Current in the Okinawa Trough induced by enhanced EASM and transition to a La Niña-like state led to the decrease in sedimentation rates and an increase in $\delta^{15}N_{sed}$ (Fig. 7a, 7c and7g).

5.3 Kuroshio and East Asian Winter Monsoon controls on primary productivity

Northeast of Taiwan, south of the Okinawa Trough, present-day measurements in surface sediments under the modern path of the Kuroshio Current observed $\delta^{15}N_{sed}$ values greater than 3‰ (Kao et al., 2003). This isotopic signature, close to those of the Taiwanese rocks (Owen, 2013; Yui et al., 2009), indicates that the signal is dominated by terrigenous inputs of nitrogen rather than by cyanobacterial activity despite the presence of *Trichodesmium* spp. in the Kuroshio Current above (Jiang et al., 2019; Liu et al., 1996). Therefore, the mere input of cyanobacteria might not be enough to explain the decrease of $\delta^{15}N_{sed}$. During LGM and HS1, the strengthened EAWM would have caused an increase in dust-borne Fe inputs as evidenced by ln(Fe/Al) (Fig. 7h), soluble iron concentration and dust mass accumulation rate in core MD06-3047 (Xu et al., 2015) (Fig. 7b). In addition a deepening of the mixed layer as observed in the northern South China Sea (Steinke et al., 2010; Zhang et al., 2016) can result in the upwelling of subsurface water. It would have caused a transfer of phosphate and nitrate from the nutrient-rich Kuroshio Current subsurface water (Chen et al., 2017, 2021, 1995) to the surface of these co-limiting nutrients (Fe, P) with consequent intensification of nitrogen fixation by cyanobacterial activity (Held et al., 2020; Lis et al., 2015; Qiu et al., 2022). This hypothesis is supported by the concomitant enhancement of nitrogen fixation in the Okinawa Trough as evidenced by the organic nitrogen $\delta^{15}N$ ($\delta^{15}N_{ON}$) of core MD01-2404 (Zheng et al.,

2015) (Fig. 7g). In the East China Sea, the nitrogen fixation is strongly related to the input of *Trichodesmium* spp. by the Kuroshio Current (Jiang et al., 2019; Liu et al., 1996; Zhang et al., 2012). This synchronous evolution (Fig. 7g) suggests that during LGM and HS1, both the remaining and deflected branches would have transported cyanobacteria northern and southern of the Okinawa Trough, and their nitrogen fixation would have been increased by an enhanced EAWM. This observation is consistent with the hypothesis of total or partial deflection from LGM to BA (Fig. 6), and highlights the control exerted by the Kuroshio Current and EAWM on nitrogen fixation in this region.

Enhanced paleoproductivity is also evidenced by the concomitant increase in ln(Br/Al), $\delta^{13}C_{org}$ and TOC (Fig. 7h – 7j) from LGM to HS1 before decreasing during and after BA. This is consistent with an enhanced EAWM winds intensity and deflection of the Kuroshio Current from LGM to BA, then a reduction of EAWM winds intensity and the collapse of the Kuroshio Current eastern branch caused by the sea level rise during and after BA (Fig. 7b and 7c). This would have resulted in the weakening of the dust-borne Fe inputs and the shallowing of the mixed layer, and the cessation of N and P supply by the Kuroshio Current subsurface waters. The impact of dust-borne Fe inputs and/or monsoonal upwelling of nutrients from the subsurface on primary productivity during LGM and HS1 is supported by previous studies in the northern South China Sea (J. He et al., 2013; Zhang et al., 2016; Zhou et al., 2016), in the Okinawa Trough (Ruan et al., 2017) and southern Philippine Sea (Xu et al., 2020, 2015), and by a modern study showing that N is the first-order limiting nutrient and P, Fe are second-order co-limiting nutrient in the study area (Browning et al., 2022). Although the impact of Kuroshio Current and EAWM on paleoproductivity can be observed in the Okinawa Trough by the biogenic silica concentration (BSi) in core KX12-3 and $\delta^{15}N_{ON}$ in core MD01-2404 (Fig. 8e and 8f), in most of these records their impact is only secondary compared with the emergence

505 of the continental shelf, remobilization/erosion of its sediments, and the migration of river
506 mouths due sea level changes (Chen et al., 2023; Lim et al., 2017; Ruan et al., 2017; Xu et al.,
507 2020) (Fig. 8d, 8g – h and 8j – 8k). East of Taiwan, the limited size of the shelf (Fig. 1a) and the
508 low impact of Taiwanese sediments on primary productivity (Wang et al., 2018) render this
509 influence negligible, explaining the discrepancies observed between paleoproductivity
510 records along the Kuroshio Current south – north transect from the east of the Philippine Sea
511 to the Okinawa Trough (Fig. 8d – 8k).

512 During HS1, $\delta^{15}N_{sed}$ is marked by a significant (p-value < 0.0001; Mann-Whitney U test
513 (Mann and Whitney, 1947)) increase from 1.8‰ (±1.7) to 2.5‰ (±1.3) (Fig. 7g) concomitant
514 with the premature decline of TN (Fig. 7k) relative to other paleoproductivity proxies
515 (ln(Br/Al), $\delta^{13}C_{org}$, TOC) (Fig. 7h – 7j). This might have been caused by the intensification of
516 water wind stress resulted due to enhanced EAWM that could have limited the development
517 of *Trichodesmium* spp. and their ability to fix atmospheric N (Breitbarth et al., 2007; Chen et
518 al., 2008; Wu et al., 2018). Thus, despite an increase in dust-Fe inputs and summer
519 temperatures above 24°C (Kim et al., 2015) consistent with *Trichodesmium* spp. ecological
520 needs (Breitbarth et al., 2007), cyanobacterial productivity declined, and so did biogenic
521 nitrogen production (7g and 7k).

522 6 Conclusion

523 A multi-proxy study of the MD18-3532 core, in the Ryukyu accretionary wedge off East
524 Taiwan, has investigated the variability of the Kuroshio Current pathway and
525 paleoproductivity during the last 26 kyr.

526 High values of sedimentation rate, the distribution of clay minerals, and the low values of
527 $\delta^{15}N_{sed}$ from 22.5 to 13.6 ka suggest a partial deflection of the Kuroshio Current along the

528 eastern edge of the Ryukyu Arc during LGM until BA, and hence a transport of (i) Taiwanese
529 suspended material and (ii) *Trichodesmium* spp. cyanobacteria to the coring site. At the same
530 time, high values of $\delta^{13}C_{org}$, ln(Br/Al), ln(Ti/Al), ln(Fe/Al), TOC, TN and the low $\delta^{15}N_{sed}$ values
531 suggest that EAWM and Kuroshio Current are the main control mechanisms on
532 paleoproductivity in the northwestern Philippine Sea during that time period. Partial
533 deflection of the Kuroshio Current provides nutrient-enriched subsurface waters that upwell
534 toward the oligotrophic surface waters by deepening the mixed layer due to intensified EAWM
535 winds, which also carry dust-borne Fe, thus creating conditions conducive to an increase of
536 primary productivity. After BA, the collapse of the eastern branch of the Kuroshio Current due
537 to sea level rise and the weakening of the EAWM leads to a decrease in the supply of sediment,
538 *Trichodesmium* spp. and nutrients to the eastern edge of the Ryukyu Arc and a shallowing of
539 the mixed layer, thus reducing primary productivity and sedimentation rates.

540 Declaration of Competing Interest

541 The authors declare that they have no known competing financial interests or personal
542 relationships that could have appeared to influence the work reported in this paper.

543 Acknowledgements

544 We would like to thank the crew and shipboard scientists of R/V *Marion* Dufresne, during
545 MD214/EAGER cruise, partially funded by the National Energy Program-Phase II (NEPII) project
546 of Ministry of Science and Technology (MOST) of Taiwan and supported by the International
547 Research Project (IRP): From Deep Earth to Extreme Events (D3E) between Centre National de
548 la Recherche Scientifique (CNRS) of France and MOST of Taiwan. We would like to thank
549 Thibaud Saos from the Centre Européen de Recherches Préhistoriques de Tautavel (EPCC),

Pierre Giresse and Wolfgang Ludwig from the CEntre de Formation et de Recherche sur les Environnements Méditerranéens (CEFREM) for useful help in analyses and discussions. The authors acknowledge the CNRS INSU-SYSTER program for financial support through the ACTEE project, and the comments of two anonymous reviewers and of the editor, that have greatly improved the original manuscript.

Data Availability

The data presented in this study are available in the Pangaea database. Fenies, Pierrick; Bassetti, Maria Angela; Vazquez Riveiros, Natalia; Menniti, Christophe; Frigola, Clément; Babonneau, Nathalie; Ratzov, Gueorgui; Hsu, Shu-Kun; Su, Chih-Chieh (publication year): XRF, carbon and nitrogen organic and isotopic geochemistry, clay mineral and grain size data from sediment core MD18-3532, eastern Taiwan, over the past 26 kyr. PANGAEA, https://doi.org/10.1594/PANGAEA.959561.

CRediT author statement

Fenies, Pierrick: conceptualization, methodology, formal analysis, writing – original draft, visualization; **Bassetti, Maria-Angela**: conceptualization, writing – review & editing, supervision, project administration, funding acquisition; **Vazquez Riveiros, Natalia**: conceptualization, writing – review & editing, supervision, project administration; **Menniti, Christophe**: validation, investigation; **Frigola, Clément**: investigation; **Babonneau, Nathalie**: resources, writing – review & editing, funding acquisition; **Ratzov, Gueorgui**: resources, writing – review & editing, funding acquisition; **Hsu, Shu-Kun**: resources, writing – review & editing, funding acquisition; **Su, Chih-Chiech**: resources, writing – review & editing, funding acquisition.

7 Figures

Table 1: AMS ^{14}C ages and instrumental error, calendar ages and error (±2σ) for sediment core MD18-3532. Radiocarbon measurements were performed on the following taxa: *Globigerinoides*, *Neogloboquadrina*, *Pulleniatina obliquiloculata* and *Globigerinita glutinata*.

Depth (cm)	AMS ^{14}C age (y)	Error (y)	Calibrated Age (ka)	Error (±2σ, ka)
15.5	3814	83	3.5	0.3
72.5	5284	67	5.4	0.2
233.5	8640	80	9.0	0.3
375.5	12066	47	13.3	0.2
550.5	12484	47	13.8	0.2
870.5	14442	53	16.6	0.3
1000.5	15235	127	17.5	0.4
1279.5	16385	158	18.8	0.4
1554.5	17815	202	20.5	0.5
1842.5	19482	239	22.4	0.4
1961.5	19687	240	22.9	0.5
2079.5	21241	277	24.3	0.6
2157.5	21562	286	24.8	0.6

Table 2: Average, standard deviation (±2σ), maximum and minimum clay mineral abundance (%) and illite crystallinity values (∆° 2θ) of core MD18-3532.

Clay mineral	Mean abundance	Standard Deviation	Maximum abundance	Minimum abundance

Illite	43	6	37	51
Chlorite	28	6	22	36
Kaolinite	10	6	0	18
Illite crystallinity	0.12	0.06	0.08	0.18

578

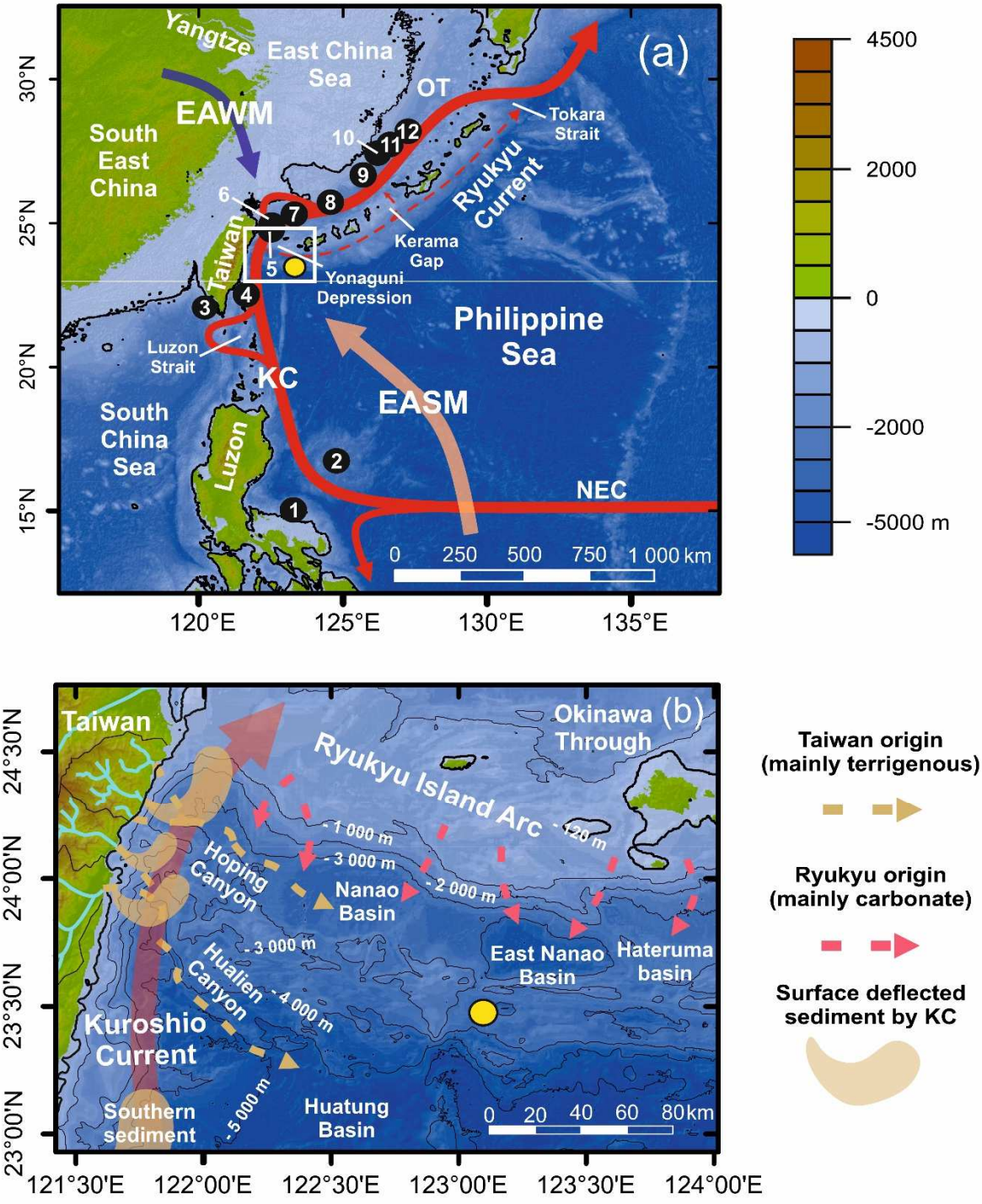

579

580 Figure 1: Maps showing (a) the modern Kuroshio Current pathway East of Taiwan and the
581 monsoon pattern in the northwestern Philippine Sea and (b) the bathymetry of the study area
582 and the different modern sedimentary sources. The yellow circle marks the position of the
583 core MD18-3532. The black circles indicate the positions of the cores MD06-3052 (1), MD06-

584 3047 (2), MD10-3291 (3), OR1715-21 (4), MD05-2908 (5), ODP 1202-B (6), core 255 (7), RN93-
585 PC6 (8), MD01-2404 (9), KX12-3 (10), M063-05 (11) and A7 (12). The 130 m isobath is marked
586 by a thicker black line and shows the emerged area at the last glacial maximum. The white
587 rectangle shows the position of the more detailed box Fig. 1b. The solid red arrow show the
588 Kuroshio Current (KC) pathway, the dotted red arrow show the Ryukyu Current pathway, the
589 blue arrow indicate the East Asian Winter Monsoon (EAWM), the orange arrow indicate the
590 East Asian Summer Monsoon (EASM). NEC: North Equatorial Current, OT: Okinawa Through.

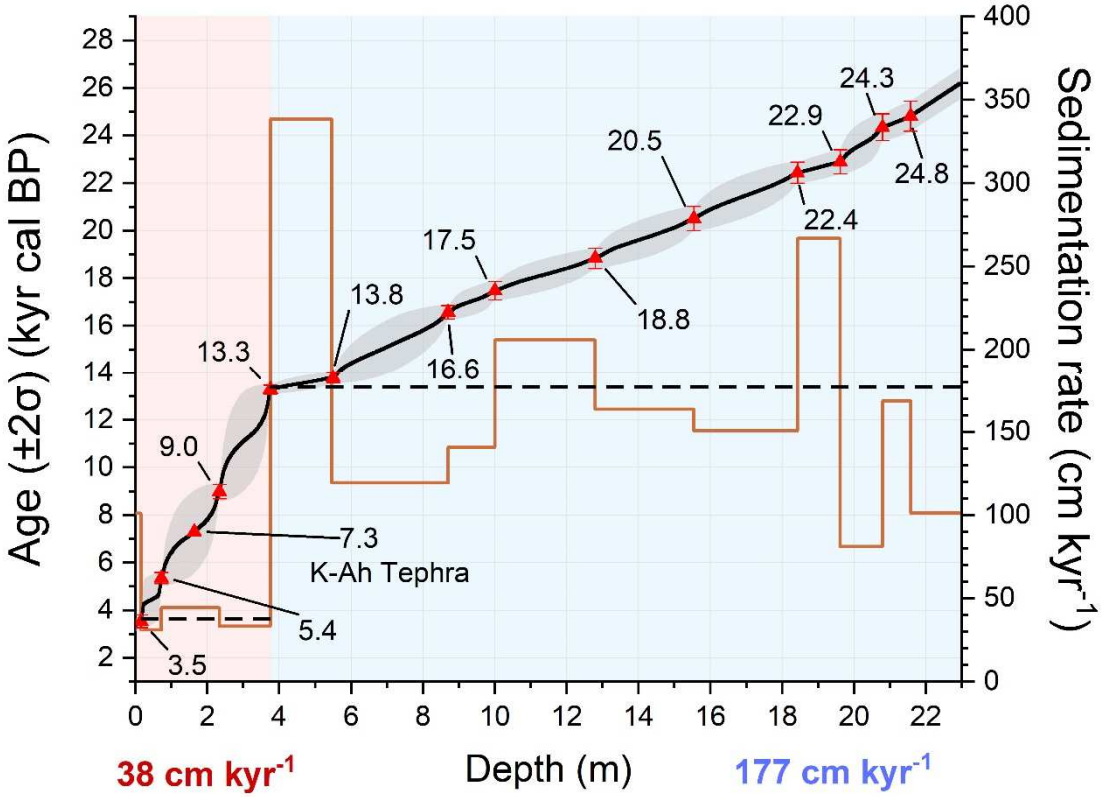

591

592 Figure 2: Age model and sedimentation rate of core MD18-3532. All dates are given in
593 calibrated radiocarbon kyr (±2σ). The black curve is the Oxcal age model and the grey area
594 shows the age model error at 2σ. The dotted lines show the average sedimentation rates from

595 3.5 to 13.3 kyr (38 cm kyr^{-1}) and from 13.3 to 24.8 kyr (177 cm kyr^{-1}). The brown curve shows

596 the evolution of the sedimentation rate in cm.kyr^{-1}.

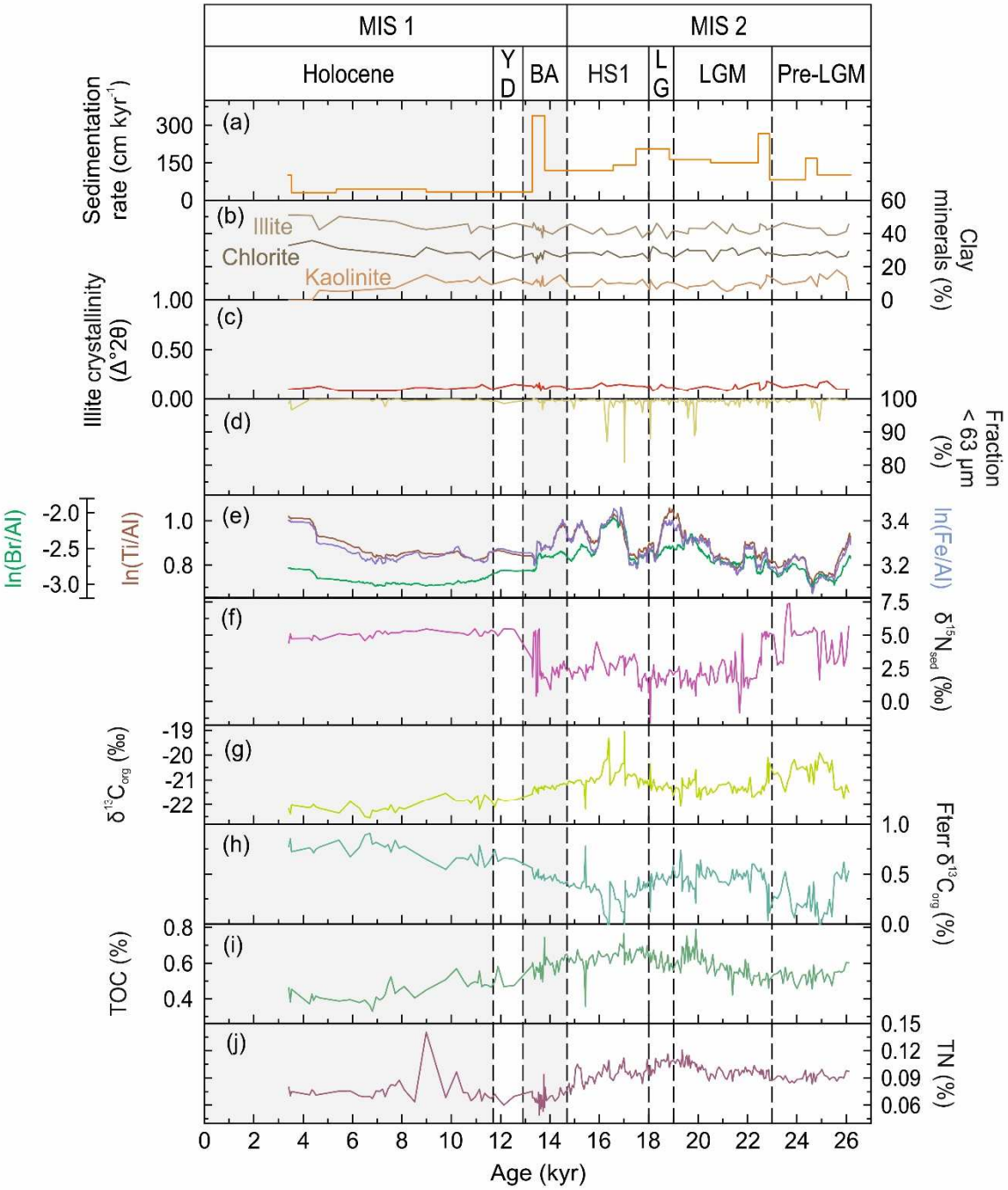

597

598 Figure 3: Results of sedimentological and geochemical measurements on core MD18-3532: (a)

599 sedimentation rate (cm kyr^{-1}), (b) clay minerals (%), (c) illite crystallinity values (Δ° 2θ), (d)

600 sediment fraction smaller than 63 µm (%), (e) elemental ratios ln(Br/Al), ln(Ti/Al) and ln(Fe/Al),

(f) $\delta^{15}N_{sed}$ (‰), (g) $\delta^{13}C_{org}$ (‰), (h) terrigenous contribution of terrestrial organic matter to $\delta^{13}C_{org}$ (%) estimated from the marine vs. continental $\delta^{13}C_{org}$ mixing model, (i) Total Organic Carbon (TOC; %), Total Nitrogen (TN; %). The division of the time scale is first done on the scale of marine isotope stages (MIS), and then on the scale of late Quaternary millennium-scale changes with: Pre-Last Glacial Maximum (Pre-LGM), Last Glacial Maximum (LGM), Late Glacial (LG), Heinrich Stadial 1 (HS1), Bølling-Allerød (BA), Younger Dryas (YD) and Holocene. Dotted lines show the limits of each millennium-scale changes and grey areas are for warming period.

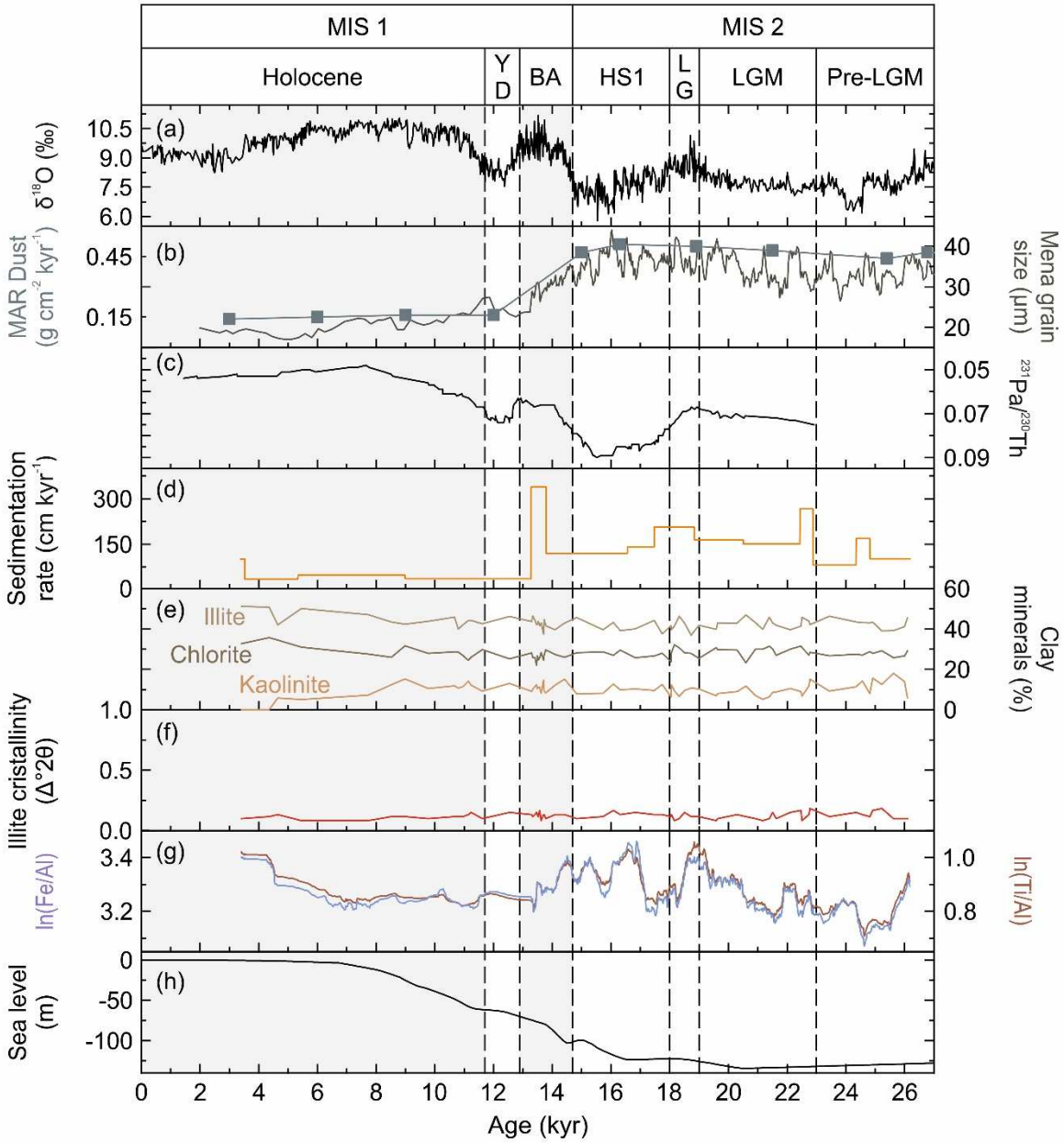

609

610 Figure 4: Evolution of terrigenous input and their origin: (a) the $\delta^{18}O$ of speleothem from Hulu
611 and Dongge caves represents the evolution of the East Asian Summer Monsoon (Cheng et al.,
612 2016), (b) Gulang Loess mean gain size (μm) (Sun et al., 2012) shows changes in the intensity
613 of the East Asian Winter Monsoon (EAWM) and dust mass accumulation rate (MAR) shows
614 the variability of the amount of dust (g cm^{-2} kyr^{-1}) brought to the ocean from the Chinese Loess
615 Plateau by the EAWM winds in core MD06-3047, east of the Philippines (Xu et al., 2015; Fig.

616 1a), (c) $^{231}Pa/^{230}Th$ shows changes in the intensity of the Atlantic Meridional Overturning
617 Circulation (McManus et al., 2004); (d) to (g) data are from core MD18-3532: (d)
618 sedimentation rate (cm kyr^{-1}), (e) percentage of clay minerals (%), (f) illite crystallinity values
619 (Δ°2θ), (g) elemental ratios ln(Fe/Al) and ln(Ti/Al); (h) relative sea level (Lambeck et al., 2014).
620 The division of the time scale is first done on the scale of marine isotope stages (MIS), and
621 then on the scale of late Quaternary millennium-scale changes with: Pre-Last Glacial
622 Maximum (Pre-LGM), Last Glacial Maximum (LGM), Late Glacial (LG), Heinrich Stadial 1 (HS1),
623 Bølling-Allerød (BA), Younger Dryas (YD) and Holocene. Dotted lines show the limits of each
624 millennium-scale changes and grey areas are for warming period.

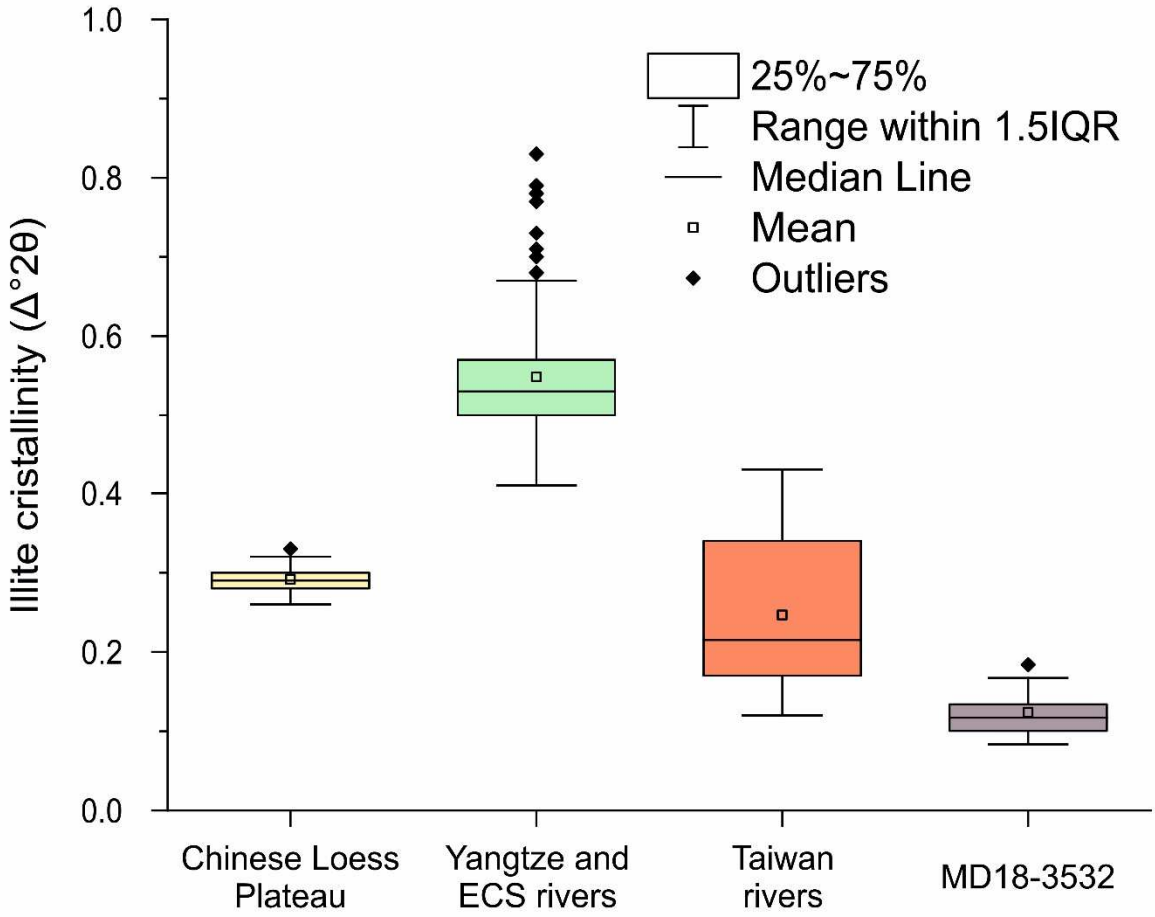

625

626 Figure 5: Illite crystallinity values (Δ°2θ) in sediments from the Chinese Loess Plateau (C. Huang
627 et al., 2011; Ji et al., 1999), the Yangtze River and East China Sea shelf (Zhao et al., 2018),
628 Taiwan rivers (Li et al., 2012; Nayak et al., 2021) and MD18-3532 (this study).

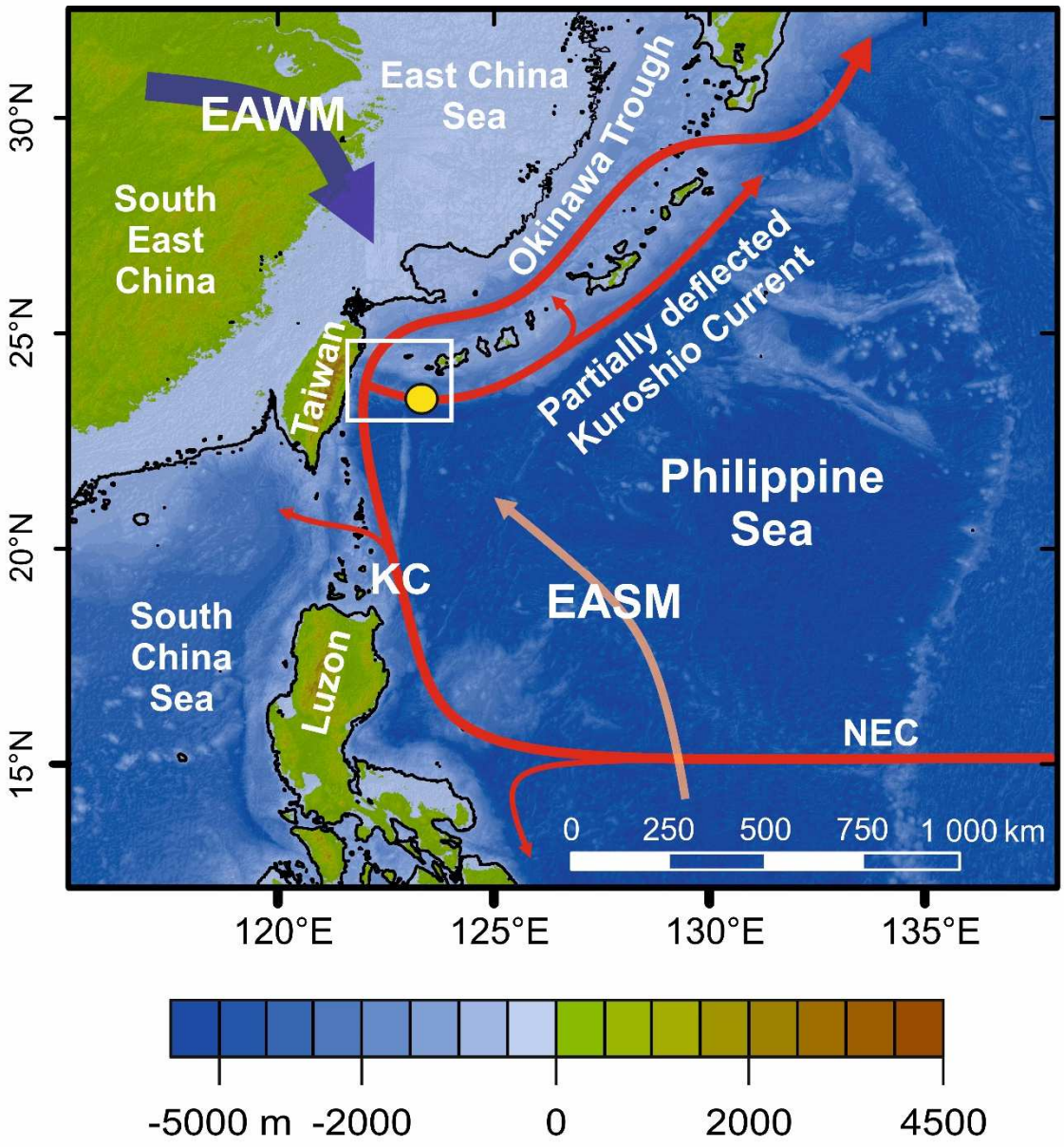

629

630 Figure 6: Proposed partial deflection of the Kuroshio Current pathway in the northwestern
631 Philippine Sea during the Last Glacial Maximum. The 130 m isobath is marked by a thicker
632 black line and shows the emerged area. NEC: North Equatrial Current, KC: Kuroshio Current,
633 EASM: East Asian Summer Monsoon, EAWM: East Asian Winter Monsoon, OT: Okinawa
634 Through.

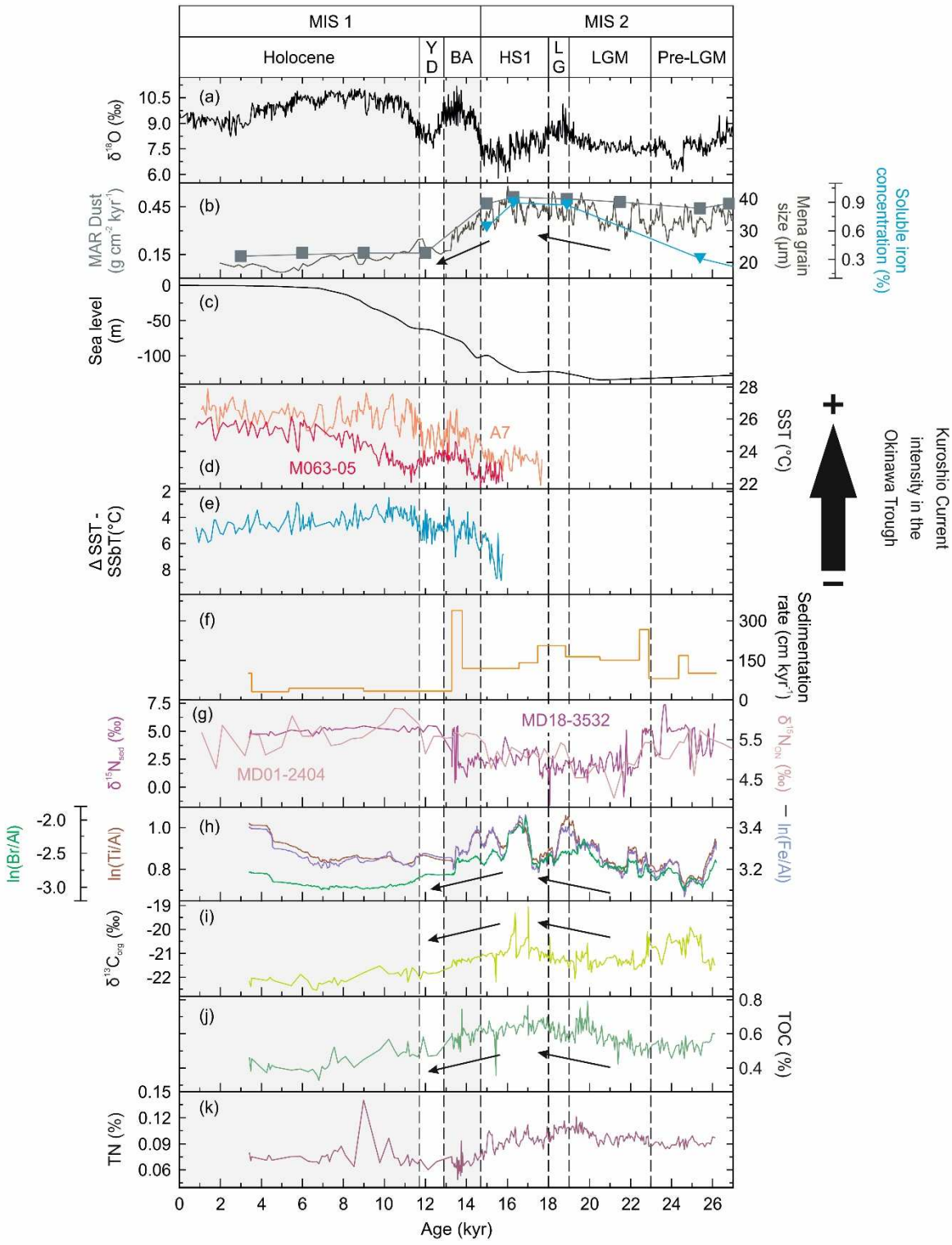

635

636 Figure 7: Variability of sedimentological and geochemical proxies with the evolution of East

637 Asian Monsoon, relative sea level and Kuroshio Current: (a) $\delta^{18}O$ of speleothems from Hulu

638 and Dongge caves represents the evolution of the East Asian Summer Monsoon (Cheng et al.,

639 2016), (b) Gulang Loess mean gain size (µm) shows changes in the intensity of the East Asian
640 Winter Monsoon (EAWM), dust mass accumulation rate (MAR) and soluble iron concentration
641 shows respectively the amount of dust (g cm^{-2} kyr^{-1}) and soluble iron (%) brought to the ocean
642 from the Chinese Loess Plateau by the EAWM winds in core MD06-3047, east of the
643 Philippines (Xu et al., 2015; Fig. 1a), (c) relative sea level (m) (Lambeck et al., 2014), (d) sea
644 surface temperature (SST) in °C respectively based on Mg/Ca and UK'_{37} measurements in core
645 A7 (red) (Sun et al., 2005) and M063-05 (orange) (Li et al., 2020) as an indicator of the Kuroshio
646 Current intensity in the middle of the Okinawa Trough (Fig. 1a), (e) relative annual mean depth
647 of the thermocline reconstituted using the temperature differences between SST and Sea
648 Subsurface Temperature (SSbT) in °C respectively based on UK'_{37} and TEX^{86}_{H} from core M063-
649 05 (Fig. 1a) as an indicator of the Kuroshio Current intensity in the middle of the Okinawa
650 Trough (Li et al., 2020). The following data are all from core MD18-3532: (f) sedimentation
651 rate (cm kyr^{-1}), (g) $\delta^{15}N_{sedimentary}$ (‰) in core MD18-3532 (this study) and $\delta^{15}N_{Organi\ Nitrogen}$ (‰)
652 in core MD01-2404 (Zheng et al., 2015; Fig. 1a), (h) elemental ratios with ln(Br/Al) indicating
653 marine organic matter; ln(Ti/Al) and ln(Fe/Al) showing eolian input of Fe and Ti by dust from
654 Chinese Plateau loess, (i) $\delta^{13}C_{org}$ (‰), (j) Total Organic Carbon (TOC; %) and (k) Total Nitrogen
655 (TN; %). The division of the time scale is first done on the scale of marine isotope stages (MIS)
656 and then on the scale of late Quaternary millennium-scale changes with: Pre-Last Glacial
657 Maximum (Pre-LGM), Last Glacial Maximum (LGM), Late Glacial (LG), Heinrich Stadial 1 (HS1),
658 Bølling-Allerød (BA), Younger Dryas (YD) and Holocene. Dotted lines show the limits of each
659 millennium-scale changes and grey areas are for warming period. Black arrows mark trends in
660 Gulang Loess mean grain size, dust mass accumulation rate and iron soluble concentration in
661 core MD06-3047 (b), elemental ratios ln(Br/Al), ln(Fe/Al) and ln(Ti/Al) (h), $\delta^{13}C_{org}$ (i) and TOC
662 (j) from the Last Glacial Maximum to the Younger Dryas.

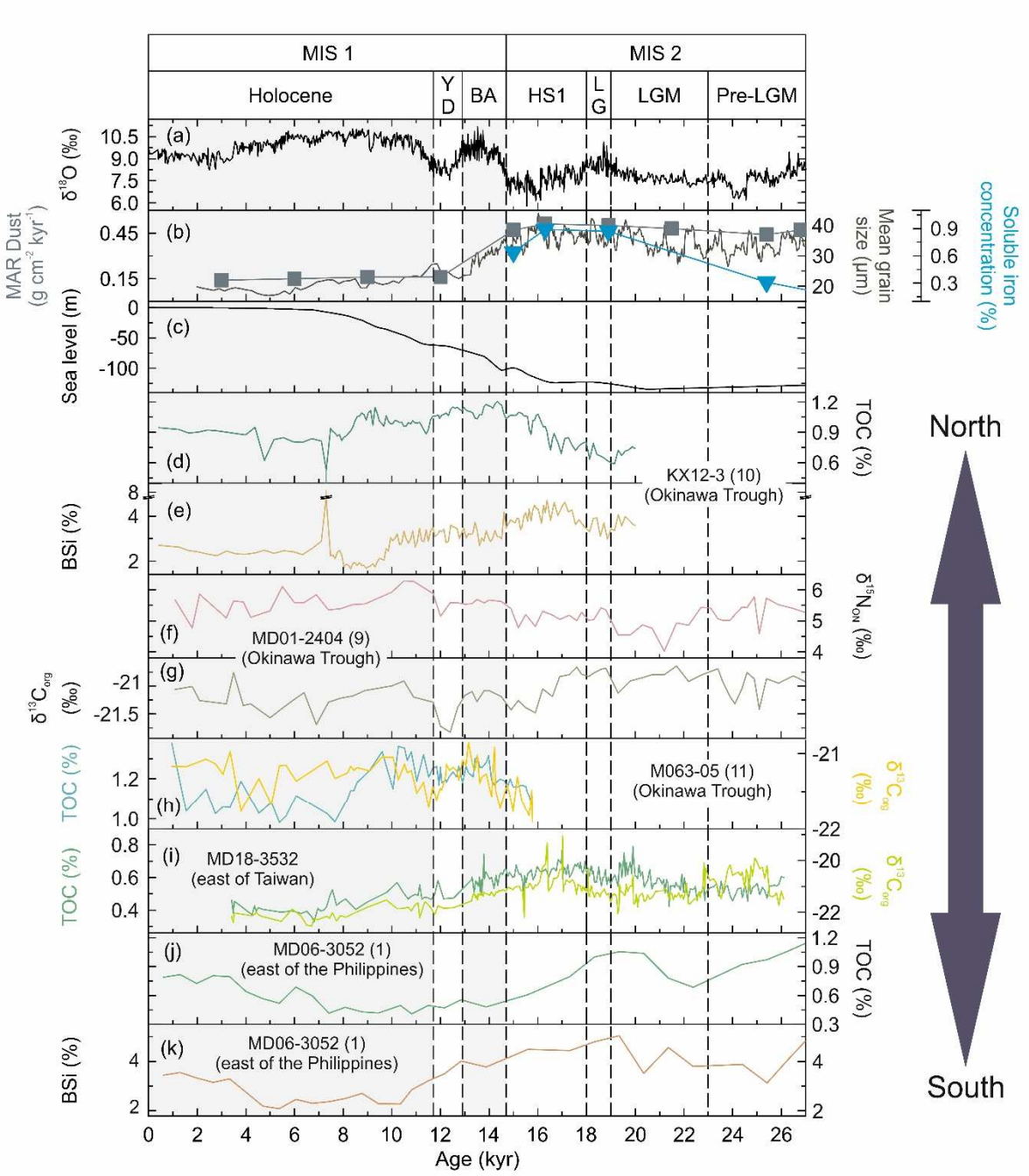

663

664 Figure 8: Spatiotemporal comparison of paleoproductivity signals along a north-south transect
665 on the path of the Kuroshio Current (Fig. 1a): (a) $\delta^{18}O$ of speleothems from Hulu and Dongge
666 caves represents the evolution of the East Asian Summer Monsoon (Cheng et al., 2016), (b)
667 Gulang Loess mean gain size (μm) shows changes in the intensity of the East Asian Winter
668 Monsoon (EAWM), dust mass accumulation rate (MAR) and soluble iron concentration shows

669 respectively the amount of dust (g cm^{-2} kyr^{-1}) and soluble iron (%) brought to the ocean from
670 the Chinese Loess Plateau by the EAWM winds in core MD06-3047, east of the Philippines (Xu
671 et al., 2015; Fig. 1a), (c) relative sea level (m) (Lambeck et al., 2014), (d) Total Organic Carbon
672 (TOC; %) in core KX12-3 (Lim et al., 2017; Fig. 1a), (e) Biogenic Silica (BSi, %) in core KX12-3
673 (Lim et al., 2017; Fig. 1a), (f) $\delta^{15}N_{Organic\ Nitrogen}$ (‰) in core MD01-2404 (Zheng et al., 2015; Fig.
674 1a), (g) $\delta^{13}C_{org}$ (‰) in core MD01-2404 (Zheng et al., 2015; Fig. 1a), (h) TOC (%) and $\delta^{13}C_{org}$ (‰)
675 in core M063-05 (Chen et al., 2023; Fig. 1a), (i) TOC (%) and $\delta^{13}C_{org}$ (‰) in core MD18-3532
676 (this study), (j) TOC (%) in core MD06-3052 (Xu et al., 2020; Fig. 1a) and (k) BSi (%) in core
677 MD06-3052 (Xu et al., 2020; Fig. 1a). Numbers in brackets after the sediment core qualifier
678 refer to the number used for core location Fig. 1a. The division of the time scale is first done
679 on the scale of marine isotope stages (MIS) and then on the scale of late Quaternary
680 millennium-scale changes with: Pre-Last Glacial Maximum (Pre-LGM), Last Glacial Maximum
681 (LGM), Late Glacial (LG), Heinrich Stadial 1 (HS1), Bølling-Allerød (BA), Younger Dryas (YD) and
682 Holocene. Dotted lines show the limits of each millennium-scale changes and grey areas are
683 for warming period.

684 # Supplementary material

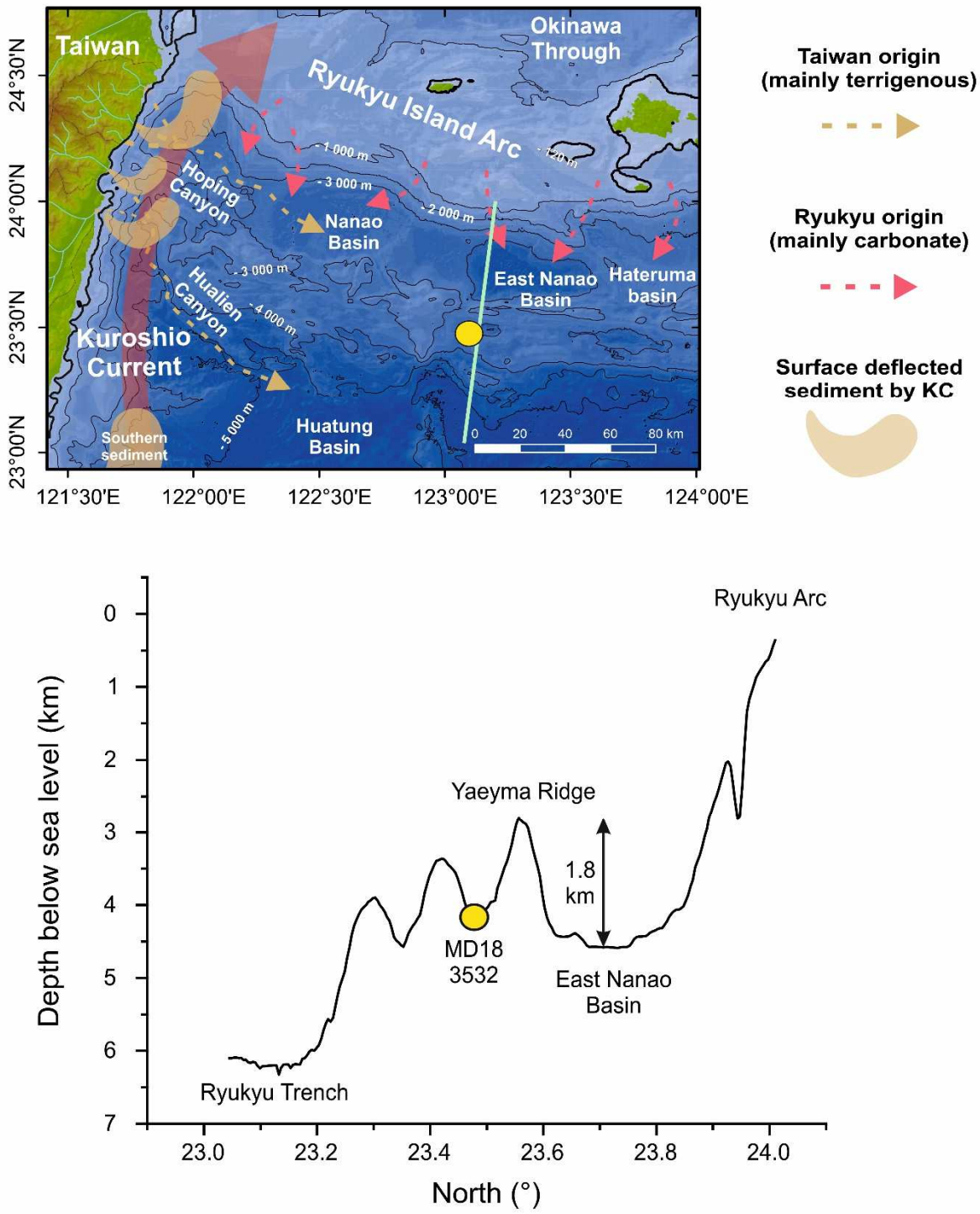

685

686 Figure S1: Bathymetric cross-section of the Ryukyu Arc up to the Ryukyu Trough represented

687 by the light green line.

Table S1: Analytical precision and accuracy of High Organic (HO) B2151 and Low Organic (LO) B2153 standards. The theoretical expected values and errors (±2σ) for $\delta^{13}C$ (‰) and $\delta^{15}N$ (‰) of the HO B2151 and LO B2153 standards are shown in the first two rows of the table. The $\delta^{13}C$ (‰) and $\delta^{15}N$ (‰) measured values of the standards and their errors are reported on the last two rows and were obtained by calculating the mean and standard deviation (±2σ) of the values measured at the beginning and end of the analysis series.

	$\delta^{13}C$ (‰)	Error (±2σ, ‰)	$\delta^{15}N$ (‰)	Error (±2σ, ‰)
HO B2151 expected	-26.27	0.15	4.42	0.29
LO B2153 expected	-26.66	0.24	7.30	0.10
HO B2151 measured	-26.31	0.21	4.43	0.49
LO B2153 measured	-26.61	0.26	7.13	0.54

Table S2: Spearman correlation matrix of ln(Br/Al), ln(Fe/Al) and ln(Ti/Al). Values in bold have a p-value < 0.05.

Variables	Br/Al	Fe/Al	Ti/Al
Br/Al	1	**0.64**	**0.65**
Fe/Al		1	**0.91**
Ti/Al			1

Table S3: Spearman correlation matrix of ln(Br/Al), ln(Fe/Al) and ln(Ti/Al) after smoothing by a 30-order moving average. Values in bold have a p-value < 0.05.

Variables	M30(Br/Al)	M30(Fe/Al)	M30(Ti/Al)
M30(Br/Al)	1	**0.74**	**0.74**
M30(Fe/Al)		1	**0.97**
M30(Ti/Al)			1

699 Table S4: Spearman correlation matrix of illite, $\delta^{15}N_{sed}$ and Total N. Values in bold have a p-
700 value < 0.05.

Variables	Illite	$\delta^{15}N_{sed}$	TN
Illite	**1**	0,1	-0,2
d15N		**1**	**-0,3**
TN			**1**

701

702 General setting – Sedimentation rate in the coastal region of Taiwan

703 The very large sediment export results in high sedimentation rate in the coastal regions of
704 Taiwan. Thus, north of Taiwan, in the southern Okinawa Through, the core MD05-2908 (5 in
705 Fig. 1a) shows a mean sedimentation rate of 500 cm.kyr^{-1} over the last 7 kyr (Li et al., 2009).
706 Nearby, the ODP site 1202B (6) shows sedimentation rate of 382 cm.kyr^{-1} in average during
707 the Holocene (Wei et al., 2005). South of Taiwan, the core MD10-3291 (3) located on the west
708 flank of the Gaoping Canyon a shows a mean sedimentation of 122 cm.kyr^{-1} over the last 12
709 kyr (Yu et al., 2017). By contrast, during the same period, areas further away from Taiwan
710 show lower sedimentation rates. For example, cores 255 (7) and RN93-PC6 (8), located further
711 north in the southern part of the Okinawa Through than the ODP 1202B and MD05-2908 sites,

have average sedimentation rates of 60 and 47 cm.kyr^{-1} (Li et al., 2009; Ujiié et al., 2003), respectively. Eastern of Taiwan, core OR1715-21 (4) located on the northern slope of the Green Island, disconnected from Taiwanese canyons inputs, shows a sedimentation rate of 25.6 cm.kyr^{-1} (Lo et al., 2013).

8 Bibliography

Addinsoft, P., 2016. XLSTAT 2016: data analysis and statistical solution for Microsoft Excel.

Breitbarth, E., Oschlies, A., LaRoche, J., 2007. Physiological constraints on the global distribution of Trichodesmium – effect of temperature on diazotrophy. Biogeosciences 4, 53–61. https://doi.org/10.5194/bg-4-53-2007

Browning, T.J., Liu, X., Zhang, R., Wen, Z., Liu, J., Zhou, Y., Xu, F., Cai, Y., Zhou, K., Cao, Z., Zhu, Y., Shi, D., Achterberg, E.P., Dai, M., 2022. Nutrient co-limitation in the subtropical Northwest Pacific. Limnol. Oceanogr. Lett. 7, 52–61. https://doi.org/10.1002/lol2.10205

Calvert, S.E., Pedersen, T.F., 2007. Chapter Fourteen Elemental Proxies for Palaeoclimatic and Palaeoceanographic Variability in Marine Sediments: Interpretation and Application, in: Developments in Marine Geology. Elsevier, pp. 567–644. https://doi.org/10.1016/S1572-5480(07)01019-6

Chamley, H., 1989. Clay Sedimentology. Springer, Berlin, Heidelberg. https://doi.org/10.1007/978-3-642-85916-8

Channell, J.E.T., Xuan, C., Hodell, D.A., Crowhurst, S.J., Larter, R.D., 2019. Relative paleointensity (RPI) and age control in Quaternary sediment drifts off the Antarctic Peninsula. Quat. Sci. Rev. 211, 17–33. https://doi.org/10.1016/j.quascirev.2019.03.006

Chen, C.-C., Jan, S., Kuo, T.-H., Li, S.-Y., 2017. Nutrient flux and transport by the Kuroshio east of Taiwan. J. Mar. Syst. 167, 43–54. https://doi.org/10.1016/j.jmarsys.2016.11.004

Chen, C.-C., Lu, C.-Y., Jan, S., Hsieh, C., Chung, C.-C., 2022. Effects of the Coastal Uplift on the Kuroshio Ecosystem, Eastern Taiwan, the Western Boundary Current of the North Pacific Ocean. Front. Mar. Sci. 9, 796187. https://doi.org/10.3389/fmars.2022.796187

Chen, C.-S., Chen, Y.-L., 2003. The Rainfall Characteristics of Taiwan. Mon. Weather Rev. 131, 1323–1341. https://doi.org/10.1175/1520-0493(2003)131<1323:TRCOT>2.0.CO;2

Chen, C.-T.A., Huang, T.-H., Wu, C.-H., Yang, H., Guo, X., 2021. Variability of the nutrient stream near Kuroshio's origin. Sci. Rep. 11, 5080. https://doi.org/10.1038/s41598-021-84420-5

Chen, C.-T.A., Liu, C.T., Pai, S.C., 1995. Variations in oxygen, nutrient and carbonate fluxes of the Kuroshio Current. La mer 33, 161–176.

Chen, J.-M., Li, T., Shih, C.-F., 2010. Tropical Cyclone– and Monsoon-Induced Rainfall Variability in Taiwan. J. Clim. 23, 4107–4120. https://doi.org/10.1175/2010JCLI3355.1

Chen, M., Li, D.-W., Li, L., Jin, G., Li, G., Xu, J., Zhao, M., 2023. Phytoplankton productivity and community structure changes in the middle Okinawa Trough since the last deglaciation. Palaeogeogr. Palaeoclimatol. Palaeoecol. 610, 111349. https://doi.org/10.1016/j.palaeo.2022.111349

753 Chen, Y., Sun, X., Zhun, M., 2018. Net-phytoplankton communities in the Western Boundary
754 Currents and their environmental correlations. J. Oceanol. Limnol. 36, 305–316.
755 https://doi.org/10.1007/s00343-017-6261-8
756 Chen, Y.L., 2000. Comparisons of primary productivity and phytoplankton size structure in the
757 marginal regions of southern East China Sea. Cont. Shelf Res. 20, 437–458.
758 https://doi.org/10.1016/S0278-4343(99)00080-1
759 Chen, Y.L., Chen, H.-Y., Tuo, S., Ohki, K., 2008. Seasonal dynamics of new production from
760 Trichodesmium N2 fixation and nitrate uptake in the upstream Kuroshio and South
761 China Sea basin. Limnol. Oceanogr. 53, 1705–1721.
762 https://doi.org/10.4319/lo.2008.53.5.1705
763 Cheng, H., Edwards, R.L., Sinha, A., Spötl, C., Yi, L., Chen, S., Kelly, M., Kathayat, G., Wang, X.,
764 Li, X., Kong, X., Wang, Y., Ning, Y., Zhang, H., 2016. The Asian monsoon over the past
765 640,000 years and ice age terminations. Nature 534, 640–646.
766 https://doi.org/10.1038/nature18591
767 Ching, K.-E., Hsieh, M.-L., Johnson, K.M., Chen, K.-H., Rau, R.-J., Yang, M., 2011. Modern
768 vertical deformation rates and mountain building in Taiwan from precise leveling and
769 continuous GPS observations, 2000–2008. J. Geophys. Res. Solid Earth 116, B08406.
770 https://doi.org/10.1029/2011JB008242
771 Clark, P.U., Shakun, J.D., Baker, P.A., Bartlein, P.J., Brewer, S., Brook, E., Carlson, A.E., Cheng,
772 H., Kaufman, D.S., Liu, Z., 2012. Global climate evolution during the last deglaciation.
773 Proc. Natl. Acad. Sci. 109, E1134–E1142. https://doi.org/10.1073/pnas.1116619109
774 Clement, A.C., Seager, R., Cane, M.A., 1999a. Orbital controls on the El Niño/Southern
775 Oscillation and the tropical climate. Paleoceanography 14, 441–456.
776 https://doi.org/10.1029/1999PA900013
777 Clement, A.C., Seager, R., Cane, M.A., 1999b. Orbital controls on the El Niño/Southern
778 Oscillation and the tropical climate. Paleoceanography 14, 441–456.
779 https://doi.org/10.1029/1999PA900013
780 Croudace, I.W., Rothwell, R.G. (Eds.), 2015. Micro-XRF Studies of Sediment Cores: Applications
781 of a non-destructive tool for the environmental sciences, Developments in
782 Paleoenvironmental Research. Springer Netherlands, Dordrecht.
783 https://doi.org/10.1007/978-94-017-9849-5
784 Dadson, S., Hovius, N., Pegg, S., Dade, W.B., Horng, M.J., Chen, H., 2005. Hyperpycnal river
785 flows from an active mountain belt. J. Geophys. Res. Earth Surf. 110, F04016.
786 https://doi.org/10.1029/2004JF000244
787 Dadson, S.J., Hovius, N., Chen, H., Dade, W.B., Hsieh, M.-L., Willett, S.D., Hu, J.-C., Horng, M.-
788 J., Chen, M.-C., Stark, C.P., Lague, D., Lin, J.-C., 2003. Links between erosion, runoff
789 variability and seismicity in the Taiwan orogen. Nature 426, 648–651.
790 https://doi.org/10.1038/nature02150
791 Das, P., Lin, A.T.-S., Chen, M.-P.P., Miramontes, E., Liu, C.-S., Huang, N.-W., Kung, J., Hsu, S.-K.,
792 Pillutla, R.K., Nayak, K., 2021. Deep-sea submarine erosion by the Kuroshio Current in
793 the Manila accretionary prism, offshore Southern Taiwan. Tectonophysics 807,
794 228813. https://doi.org/10.1016/j.tecto.2021.228813
795 Denton, G.H., Anderson, R.F., Toggweiler, J.R., Edwards, R.L., Schaefer, J.M., Putnam, A.E.,
796 2010. The Last Glacial Termination. Science 328, 1652–1656.
797 https://doi.org/10.1126/science.1184119
798 Dezileau, L., Lehu, R., Lallemand, S., Hsu, S.-K., Babonneau, N., Ratzov, G., Lin, A.T., Dominguez,
799 S., 2016. Historical Reconstruction of Submarine Earthquakes Using ^{210} Pb, ^{137} Cs, and

^{241} Am Turbidite Chronology and Radiocarbon Reservoir Age Estimation off East Taiwan. Radiocarbon 58, 25–36. https://doi.org/10.1017/RDC.2015.3
Diekmann, B., Hofmann, J., Henrich, R., Fütterer, D.K., Röhl, U., Wei, K.-Y., 2008. Detrital sediment supply in the southern Okinawa Trough and its relation to sea-level and Kuroshio dynamics during the late Quaternary. Mar. Geol. 255, 83–95. https://doi.org/10.1016/j.margeo.2008.08.001
Dong, J., Li, A., Liu, X., Wan, S., Xu, F., Shi, X., 2020. Holocene Climate Modulates Mud Supply, Transport, and Sedimentation on the East China Sea Shelf. J. Geophys. Res. Earth Surf. 125, e2020JF005731. https://doi.org/10.1029/2020JF005731
Dou, Y., Yang, S., Liu, Z., Clift, P.D., Yu, H., Berne, S., Shi, X., 2010. Clay mineral evolution in the central Okinawa Trough since 28ka: Implications for sediment provenance and paleoenvironmental change. Palaeogeogr. Palaeoclimatol. Palaeoecol. 288, 108–117. https://doi.org/10.1016/j.palaeo.2010.01.040
Dou, Y., Yang, S., Liu, Z., Shi, X., Li, J., Yu, H., Berne, S., 2012. Sr–Nd isotopic constraints on terrigenous sediment provenances and Kuroshio Current variability in the Okinawa Trough during the late Quaternary. Palaeogeogr. Palaeoclimatol. Palaeoecol. 365–366, 38–47. https://doi.org/10.1016/j.palaeo.2012.09.003
Eberl, R., Carpenter, E., 2007. Association of the copepod Macrosetella gracilis with the cyanobacterium Trichodesmium spp. in the North Pacific Gyre. Mar. Ecol. Prog. Ser. 333, 205–212. https://doi.org/10.3354/meps333205
Ford, H.L., Ravelo, A.C., Polissar, P.J., 2015. Reduced El Niño–Southern Oscillation during the Last Glacial Maximum. Science 347, 255–258. https://doi.org/10.1126/science.1258437
Fujiwara, K., Kawamura, R., Kawano, T., 2020. Remote Thermodynamic Impact of the Kuroshio Current on a Developing Tropical Cyclone Over the Western North Pacific in Boreal Fall. J. Geophys. Res. Atmospheres 125, e2019JD031356. https://doi.org/10.1029/2019JD031356
Galbraith, E.D., Kienast, M., Jaccard, S.L., Pedersen, T.F., Brunelle, B.G., Sigman, D.M., Kiefer, T., 2008. Consistent relationship between global climate and surface nitrate utilization in the western subarctic Pacific throughout the last 500 ka. Paleoceanography 23, PA2212. https://doi.org/10.1029/2007PA001518
Goericke, R., Fry, B., 1994. Variations of marine plankton δ13C with latitude, temperature, and dissolved CO2 in the world ocean. Glob. Biogeochem. Cycles 8, 85–90. https://doi.org/10.1029/93GB03272
Govin, A., Holzwarth, U., Heslop, D., Ford Keeling, L., Zabel, M., Mulitza, S., Collins, J.A., Chiessi, C.M., 2012. Distribution of major elements in Atlantic surface sediments (36°N–49°S): Imprint of terrigenous input and continental weathering. Geochem. Geophys. Geosystems 13. https://doi.org/10.1029/2011GC003785
Gray, W.M., 1977. Tropical cyclone genesis in the western North Pacific. J. Meteorol. Soc. Jpn. Ser II 55, 465–482.
Guo, X., Zhu, X.-H., Wu, Q.-S., Huang, D., 2012. The Kuroshio nutrient stream and its temporal variation in the East China Sea. J. Geophys. Res. Oceans 117. https://doi.org/10.1029/2011JC007292
Harvey, G.R., 1980. A study of the chemistry of iodine and bromine in marine sediments. Mar. Chem. 8, 327–332. https://doi.org/10.1016/0304-4203(80)90021-3
He, J., Zhao, M., Wang, P., Li, L., Li, Q., 2013. Changes in phytoplankton productivity and community structure in the northern South China Sea during the past 260ka.

Palaeogeogr. Palaeoclimatol. Palaeoecol. 392, 312–323. https://doi.org/10.1016/j.palaeo.2013.09.010
He, M., Zheng, H., Huang, X., Jia, J., Li, L., 2013. Yangtze River sediments from source to sink traced with clay mineralogy. J. Asian Earth Sci., New Global Perspectives on Paleontology, Stratigraphy, Paleoceanography, Paleoclimatology, and Tectonics in the East Asia and Western Pacific 69, 60–69. https://doi.org/10.1016/j.jseaes.2012.10.001
He, S., Cheng, X., Fei, J., Wei, Z., Huang, X., Liu, L., 2022. Thermal Response to Tropical Cyclones Over the Kuroshio. Earth Space Sci. 9, e2021EA002001. https://doi.org/10.1029/2021EA002001
Heaton, T.J., Köhler, P., Butzin, M., Bard, E., Reimer, R.W., Austin, W.E.N., Bronk Ramsey, C., Grootes, P.M., Hughen, K.A., Kromer, B., Reimer, P.J., Adkins, J., Burke, A., Cook, M.S., Olsen, J., Skinner, L.C., 2020. Marine20—The Marine Radiocarbon Age Calibration Curve (0–55,000 cal BP). Radiocarbon 62, 779–820. https://doi.org/10.1017/RDC.2020.68
Held, N.A., Webb, E.A., McIlvin, M.M., Hutchins, D.A., Cohen, N.R., Moran, D.M., Kunde, K., Lohan, M.C., Mahaffey, C., Woodward, E.M.S., Saito, M.A., 2020. Co-occurrence of Fe and P stress in natural populations of the marine diazotroph *Trichodesmium*. Biogeosciences 17, 2537–2551. https://doi.org/10.5194/bg-17-2537-2020
Hillenbrand, C.-D., Crowhurst, S.J., Williams, M., Hodell, D.A., McCave, I.N., Ehrmann, W., Xuan, C., Piotrowski, A.M., Hernández-Molina, F.J., Graham, A.G.C., Grobe, H., Williams, T.J., Horrocks, J.R., Allen, C.S., Larter, R.D., 2021. New insights from multi-proxy data from the West Antarctic continental rise: Implications for dating and interpreting Late Quaternary palaeoenvironmental records. Quat. Sci. Rev. 257, 106842. https://doi.org/10.1016/j.quascirev.2021.106842
Hilton, R.G., Galy, A., Hovius, N., Horng, M.-J., Chen, H., 2010. The isotopic composition of particulate organic carbon in mountain rivers of Taiwan. Geochim. Cosmochim. Acta 74, 3164–3181. https://doi.org/10.1016/j.gca.2010.03.004
Ho, C.S., 1986. A synthesis of the geologic evolution of Taiwan. Tectonophysics, Geodynamics of the Eurasia\3-Philippine Sea Plate Boundary 125, 1–16. https://doi.org/10.1016/0040-1951(86)90004-1
Hollstein, M., Mohtadi, M., Rosenthal, Y., Prange, M., Oppo, D.W., Martínez Méndez, G., Tachikawa, K., Moffa Sanchez, P., Steinke, S., Hebbeln, D., 2018. Variations in Western Pacific Warm Pool surface and thermocline conditions over the past 110,000 years: Forcing mechanisms and implications for the glacial Walker circulation. Quat. Sci. Rev. 201, 429–445. https://doi.org/10.1016/j.quascirev.2018.10.030
Horng, C.S., Huh, C.A., Chen, K.H., Lin, C.H., Shea, K.S., Hsiung, K.H., 2012. Pyrrhotite as a tracer for denudation of the Taiwan orogen. Geochem. Geophys. Geosystems 13, undefined-undefined. https://doi.org/10.1029/2012GC004195
Hsiung, K.-H., Kanamatsu, T., Ikehara, K., Shiraishi, K., Horng, C.-S., Usami, K., 2017. Morpho-sedimentary features and sediment dispersal systems of the southwest end of the Ryukyu Trench: a source-to-sink approach. Geo-Mar. Lett. 37, 561–577. https://doi.org/10.1007/s00367-017-0509-3
Hsu, Y.-J., Lai, Y.-R., You, R.-J., Chen, H.-Y., Teng, L.S., Tsai, Y.-C., Tang, C.-H., Su, H.-H., 2018. Detecting rock uplift across southern Taiwan mountain belt by integrated GPS and leveling data. Tectonophysics 744, 275–284. https://doi.org/10.1016/j.tecto.2018.07.012

Hu, D., Wu, L., Cai, W., Gupta, A.S., Ganachaud, A., Qiu, B., Gordon, A.L., Lin, X., Chen, Z., Hu, S., Wang, G., Wang, Q., Sprintall, J., Qu, T., Kashino, Y., Wang, F., Kessler, W.S., 2015. Pacific western boundary currents and their roles in climate. Nature 522, 299–308. https://doi.org/10.1038/nature14504

Huang, C., Zhao, W., Liu, F., Tan, W., Koopal, L.K., 2011. Environmental significance of mineral weathering and pedogenesis of loess on the southernmost Loess Plateau, China. Geoderma 163, 219–226. https://doi.org/10.1016/j.geoderma.2011.04.018

Huang, E., Tian, J., Steinke, S., 2011. Millennial-scale dynamics of the winter cold tongue in the southern South China Sea over the past 26ka and the East Asian winter monsoon. Quat. Res. 75, 196–204. https://doi.org/10.1016/j.yqres.2010.08.014

Jaboyedoff, M., Bussy, F., Kübler, B., Thelin, Ph., 2001. Illite "Crystallinity" Revisited. Clays Clay Miner. 49, 156–167. https://doi.org/10.1346/CCMN.2001.0490205

Jan, S., Yang, Y.J., Wang, J., Mensah, V., Kuo, T.-H., Chiou, M.-D., Chern, C.-S., Chang, M.-H., Chien, H., 2015. Large variability of the Kuroshio at 23.75°N east of Taiwan. J. Geophys. Res. Oceans 120, 1825–1840. https://doi.org/10.1002/2014JC010614

Ji, J., Chen, J., Lu, H., 1999. Origin of illite in the loess from the Luochuan area, Loess Plateau, Central China. Clay Miner. 34, 525–532. https://doi.org/10.1180/000985599546398

Jiang, F., Zhou, Ye, Nan, Q., Zhou, Yu, Zheng, X., Li, T., Li, A., Wang, H., 2016. Contribution of Asian dust and volcanic material to the western Philippine Sea over the last 220 kyr as inferred from grain size and Sr-Nd isotopes: DUST AND VOLCANIC MATERIAL CONTRIBUTION. J. Geophys. Res. Oceans 121, 6911–6928. https://doi.org/10.1002/2016JC012000

Jiang, Z., Chen, J., Zhai, H., Zhou, F., Yan, X., Zhu, Y., Xuan, J., Shou, L., Chen, Q., 2019. Kuroshio Shape Composition and Distribution of Filamentous Diazotrophs in the East China Sea and Southern Yellow Sea. J. Geophys. Res. Oceans 124, 7421–7436. https://doi.org/10.1029/2019JC015413

Kandasamy, S., Lin, B., Lou, J.-Y., Kao, S.-J., Chen, C.-T.A., Mayer, L.M., 2018. Estimation of Marine Versus Terrigenous Organic Carbon in Sediments Off Southwestern Taiwan Using the Bromine to Total Organic Carbon Ratio as a Proxy. J. Geophys. Res. Biogeosciences 123, 3387–3402. https://doi.org/10.1029/2018JG004674

Kao, S.-J., Hilton, R.G., Selvaraj, K., Dai, M., Zehetner, F., Huang, J.-C., Hsu, S.-C., Sparkes, R., Liu, J.T., Lee, T.-Y., Yang, J.-Y.T., Galy, A., Xu, X., Hovius, N., 2014. Preservation of terrestrial organic carbon in marine sediments offshore Taiwan: mountain building and atmospheric carbon dioxide sequestration. Earth Surf. Dyn. 2, 127–139. https://doi.org/10.5194/esurf-2-127-2014

Kao, S.J., Lin, F.J., Liu, K.K., 2003. Organic carbon and nitrogen contents and their isotopic compositions in surficial sediments from the East China Sea shelf and the southern Okinawa Trough. Deep Sea Res. Part II Top. Stud. Oceanogr., Circulation and biogeochemical processes in the East China Sea and the vicinity of Taiwan 50, 1203–1217. https://doi.org/10.1016/S0967-0645(03)00018-3

Kim, R.A., Lee, K.E., Bae, S.W., 2015. Sea surface temperature proxies (alkenones, foraminiferal Mg/Ca, and planktonic foraminiferal assemblage) and their implications in the Okinawa Trough. Prog. Earth Planet. Sci. 2, 43. https://doi.org/10.1186/s40645-015-0074-1

Kim, S., Khim, B.-K., Ikehara, M., Takahashi, K., 2017. Relationship between δ15N values of bulk sediments and total organic carbon concentration in response to orbital-scale biogenic opal production in the Bering slope area over the last 600 kyrs. Quat. Int.,

940 Marine Geology in Asian Marginal Seas: ICAMG-8 459, 144–152.
941 https://doi.org/10.1016/j.quaint.2017.05.041
942 Kneller, B., Buckee, C., 2000. The structure and fluid mechanics of turbidity currents: a review
943 of some recent studies and their geological implications. Sedimentology 47, 62–94.
944 https://doi.org/10.1046/j.1365-3091.2000.047s1062.x
945 Kodama, T., Shimizu, Y., Ichikawa, T., Hiroe, Y., Kusaka, A., Morita, H., Shimizu, M., Hidaka, K.,
946 2014. Seasonal and spatial contrast in the surface layer nutrient content around the
947 Kuroshio along 138°E, observed between 2002 and 2013. J. Oceanogr. 70, 489–503.
948 https://doi.org/10.1007/s10872-014-0245-5
949 Koutavas, A., Lynch-Stieglitz, J., Marchitto, T.M., Sachs, J.P., 2002. El Niño-Like Pattern in Ice
950 Age Tropical Pacific Sea Surface Temperature. Science 297, 226–230.
951 https://doi.org/10.1126/science.1072376
952 Kutzbach, J.E., 1993. Simulated climatic changes: results of the COHMAP climate-model
953 experiments. Glob. Clim. Last Glacial Maximum 24–93.
954 Lambeck, K., Rouby, H., Purcell, A., Sun, Y., Sambridge, M., 2014. Sea level and global ice
955 volumes from the Last Glacial Maximum to the Holocene. Proc. Natl. Acad. Sci. 111,
956 15296–15303. https://doi.org/10.1073/pnas.1411762111
957 Li, C., Jiang, B., Li, A., Li, T., Jiang, F., 2009. Sedimentation rates and provenance analysis in the
958 Southwestern Okinawa Trough since the mid-Holocene. Sci. Bull. 54, 1234–1242.
959 https://doi.org/10.1007/s11434-009-0010-0
960 Li, C., Shi, X., Kao, S., Chen, M., Liu, Y., Fang, X., Lü, H., Zou, J., Liu, S., Qiao, S., 2012. Clay mineral
961 composition and their sources for the fluvial sediments of Taiwanese rivers. Chin. Sci.
962 Bull. 57, 673–681. https://doi.org/10.1007/s11434-011-4824-1
963 Li, C.-F., Chytry, M., Zelený, D., Chen, J.-J., Chen, T.-Y., Chiou, C.-R., Hsia, Y., Liu, H.-Y., Sheng-
964 Zehn, Y., Yeh, C., Wang, J.-C., Yu, C.-F., Lai, Y.-J., Chao, W.-C., Hsieh, C.-F., 2013.
965 Classification of Taiwan forest vegetation. Appl. Veg. Sci. 16, 698–719.
966 https://doi.org/10.1111/avsc.12025
967 Li, Q., Li, G., Chen, M.-T., Xu, J., Liu, S., Chen, M., 2020. New Insights Into Kuroshio Current
968 Evolution Since the Last Deglaciation Based on Paired Organic Paleothermometers
969 From the Middle Okinawa Trough. Paleoceanogr. Paleoclimatology 35,
970 e2020PA004140. https://doi.org/10.1029/2020PA004140
971 Li, Q., Zhang, Q., Li, G., Liu, Q., Chen, M.-T., Xu, J., Li, J., 2019. A new perspective for the
972 sediment provenance evolution of the middle Okinawa Trough since the last
973 deglaciation based on integrated methods. Earth Planet. Sci. Lett. 528, 115839.
974 https://doi.org/10.1016/j.epsl.2019.115839
975 Lim, D., Kim, J., Xu, Z., Jeong, K., Jung, H., 2017. New evidence for Kuroshio inflow and
976 deepwater circulation in the Okinawa Trough, East China Sea: Sedimentary mercury
977 variations over the last 20 kyr. Paleoceanography 32, 571–579.
978 https://doi.org/10.1002/2017PA003116
979 Lis, H., Kranzler, C., Keren, N., Shaked, Y., 2015. A Comparative Study of Iron Uptake Rates and
980 Mechanisms amongst Marine and Fresh Water Cyanobacteria: Prevalence of
981 Reductive Iron Uptake. Life 5, 841–860. https://doi.org/10.3390/life5010841
982 Liu, J., Xiang, R., Kao, S.-J., Fu, S., Zhou, L., 2016. Sedimentary responses to sea-level rise and
983 Kuroshio Current intrusion since the Last Glacial Maximum: Grain size and clay mineral
984 evidence from the northern South China Sea slope. Palaeogeogr. Palaeoclimatol.
985 Palaeoecol. 450, 111–121. https://doi.org/10.1016/j.palaeo.2016.03.002

Liu, J.P., Li, A.C., Xu, K.H., Velozzi, D.M., Yang, Z.S., Milliman, J.D., DeMaster, D.J., 2006. Sedimentary features of the Yangtze River-derived along-shelf clinoform deposit in the East China Sea. Cont. Shelf Res., Special Issue in Honor of Richard W. Sternberg's Contributions to Marine Sedimentology 26, 2141–2156. https://doi.org/10.1016/j.csr.2006.07.013

Liu, K.-K., Su, M.-J., Hsueh, C.-R., Gong, G.-C., 1996. The nitrogen isotopic composition of nitrate in the Kuroshio Water northeast of Taiwan: evidence for nitrogen fixation as a source of isotopically light nitrate. Mar. Chem. 54, 273–292. https://doi.org/10.1016/0304-4203(96)00034-5

Liu, X., Wei, J., 2015. Understanding surface and subsurface temperature changes induced by tropical cyclones in the Kuroshio. Ocean Dyn. 65, 1017–1027. https://doi.org/10.1007/s10236-015-0851-9

Liu, Z., Colin, C., Li, X., Zhao, Y., Tuo, S., Chen, Z., Siringan, F.P., Liu, J.T., Huang, C.-Y., You, C.-F., Huang, K.-F., 2010. Clay mineral distribution in surface sediments of the northeastern South China Sea and surrounding fluvial drainage basins: Source and transport. Mar. Geol. 277, 48–60. https://doi.org/10.1016/j.margeo.2010.08.010

Lo, L., Lai, Y.-H., Wei, K.-Y., Lin, Y.-S., Mii, H.-S., Shen, C.-C., 2013. Persistent sea surface temperature and declined sea surface salinity in the northwestern tropical Pacific over the past 7500years. J. Asian Earth Sci. 66, 234–239. https://doi.org/10.1016/j.jseaes.2013.01.014

Maher, B.A., 2016. Palaeoclimatic records of the loess/palaeosol sequences of the Chinese Loess Plateau. Quat. Sci. Rev. 154, 23–84. https://doi.org/10.1016/j.quascirev.2016.08.004

Mann, H.B., Whitney, D.R., 1947. On a test of whether one of two random variables is stochastically larger than the other. Ann. Math. Stat. 50–60.

Martinez-Ruiz, F., Kastner, M., Gallego-Torres, D., Rodrigo-Gámiz, M., Nieto-Moreno, V., Ortega-Huertas, M., 2015. Paleoclimate and paleoceanography over the past 20,000 yr in the Mediterranean Sea Basins as indicated by sediment elemental proxies. Quat. Sci. Rev. 107, 25–46. https://doi.org/10.1016/j.quascirev.2014.09.018

Matsu'ura, T., Ikehara, M., Ueno, T., 2021. Late Quaternary tephrostratigraphy and cryptotephrostratigraphy of core MD012422: Improving marine tephrostratigraphy of the NW Pacific. Quat. Sci. Rev. 257, 106808. https://doi.org/10.1016/j.quascirev.2021.106808

Mayer, L.M., Schick, L.L., Allison, M.A., Ruttenberg, K.C., Bentley, S.J., 2007. Marine vs. terrigenous organic matter in Louisiana coastal sediments: The uses of bromine:organic carbon ratios. Mar. Chem. 107, 244–254. https://doi.org/10.1016/j.marchem.2007.07.007

McGee, D., Moreno-Chamarro, E., Marshall, J., Galbraith, E.D., 2018. Western U.S. lake expansions during Heinrich stadials linked to Pacific Hadley circulation. Sci. Adv. 4, eaav0118. https://doi.org/10.1126/sciadv.aav0118

McManus, J.F., Francois, R., Gherardi, J.-M., Keigwin, L.D., Brown-Leger, S., 2004. Collapse and rapid resumption of Atlantic meridional circulation linked to deglacial climate changes. Nature 428, 834–837. https://doi.org/10.1038/nature02494

Merkel, U., Prange, M., Schulz, M., 2010. ENSO variability and teleconnections during glacial climates. Quat. Sci. Rev., Climate of the Last Million Years: New Insights from EPICA and Other Records 29, 86–100. https://doi.org/10.1016/j.quascirev.2009.11.006

Meyers, P.A., 1997. Organic geochemical proxies of paleoceanographic, paleolimnologic, and paleoclimatic processes. Org. Geochem. 27, 213–250. https://doi.org/10.1016/S0146-6380(97)00049-1

Mix, A.C., Bard, E., Schneider, R., 2001. Environmental processes of the ice age: land, oceans, glaciers (EPILOG). Quat. Sci. Rev. 20, 627–657. https://doi.org/10.1016/S0277-3791(00)00145-1

Mulder, T., Syvitski, J.P.M., Migeon, S., Faugères, J.-C., Savoye, B., 2003. Marine hyperpycnal flows: initiation, behavior and related deposits. A review. Mar. Pet. Geol. 20, 861–882. https://doi.org/10.1016/j.marpetgeo.2003.01.003

Na, H., Wimbush, M., Park, J.-H., Nakamura, H., Nishina, A., 2014. Observations of flow variability through the Kerama Gap between the East China Sea and the Northwestern Pacific. J. Geophys. Res. Oceans 119, 689–703. https://doi.org/10.1002/2013JC008899

Nayak, K., Garzanti, E., Lin, A.T.-S., Castelltort, S., 2022. Taiwan river muds from source to sink: Provenance control, inherited weathering, and offshore dispersal pathways. Sediment. Geol. 438, 106199. https://doi.org/10.1016/j.sedgeo.2022.106199

Nayak, K., Lin, A.T.-S., Huang, K.-F., Liu, Z., Babonneau, N., Ratzov, G., Pillutla, R.K., Das, P., Hsu, S.-K., 2021. Clay-mineral distribution in recent deep-sea sediments around Taiwan: Implications for sediment dispersal processes. Tectonophysics 814, 228974. https://doi.org/10.1016/j.tecto.2021.228974

Nieto-Moreno, V., Martínez-Ruiz, F., Giralt, S., Jiménez-Espejo, F., Gallego-Torres, D., Rodrigo-Gámiz, M., García-Orellana, J., Ortega-Huertas, M., de Lange, G.J., 2011. Tracking climate variability in the western Mediterranean during the Late Holocene: a multiproxy approach. Clim. Past 7, 1395–1414. https://doi.org/10.5194/cp-7-1395-2011

Owen, J.S., 2013. Stable Nitrogen Isotopes in a Forested Watershed in Taiwan. J. For. Environ. Sci. 29, 116–124. https://doi.org/10.7747/JFS.2013.29.2.116

Pan, J., Feng, X., Lai, W., Devlin, A.T., Lin, H., 2018. Barrier Effects of the Kuroshio Current on the East Asian Northerly Monsoon: A Sensitivity Analysis. Sci. Rep. 8, 18044. https://doi.org/10.1038/s41598-018-36577-9

Qiu, B., 2001. Kuroshio And Oyashio Currents, in: Encyclopedia of Ocean Sciences. Elsevier, pp. 1413–1425. https://doi.org/10.1006/rwos.2001.0350

Qiu, B., Lukas, R., 1996. Seasonal and interannual variability of the North Equatorial Current, the Mindanao Current, and the Kuroshio along the Pacific western boundary. J. Geophys. Res. Oceans 101, 12315–12330. https://doi.org/10.1029/95JC03204

Qiu, B., Rudnick, D.L., Cerovecki, I., Cornuelle, B.D., Chen, S., Schönau, M.C., McClean, J.L., Gopalakrishnan, G., 2015. The Pacific North Equatorial Current: New Insights from the Origins of the Kuroshio and Mindanao Currents (OKMC) Project. Oceanography 28, 24–33. http://dx.doi.org/10.5670/oceanog.2015.78

Qiu, G.-W., Koedooder, C., Qiu, B.-S., Shaked, Y., Keren, N., 2022. Iron transport in cyanobacteria – from molecules to communities. Trends Microbiol. 30, 229–240. https://doi.org/10.1016/j.tim.2021.06.001

Qu, T., Lukas, R., 2003. The Bifurcation of the North Equatorial Current in the Pacific. J. Phys. Oceanogr. 33, 5–18. https://doi.org/10.1175/1520-0485(2003)033<0005:TBOTNE>2.0.CO;2

Ramsey, C.B., 2008. Deposition models for chronological records. Quat. Sci. Rev., INTegration of Ice-core, Marine and Terrestrial records (INTIMATE): Refining the record of the Last

Glacial-Interglacial Transition 27, 42–60. https://doi.org/10.1016/j.quascirev.2007.01.019
Resentini, A., Goren, L., Castelltort, S., Garzanti, E., 2017. Partitioning sediment flux by provenance and tracing erosion patterns in Taiwan. J. Geophys. Res. Earth Surf. 122, 1430–1454. https://doi.org/10.1002/2016JF004026
Richter, T.O., van der Gaast, S., Koster, B., Vaars, A., Gieles, R., de Stigter, H.C., De Haas, H., van Weering, T.C.E., 2006. The Avaatech XRF Core Scanner: technical description and applications to NE Atlantic sediments. Geol. Soc. Lond. Spec. Publ. 267, 39–50. https://doi.org/10.1144/GSL.SP.2006.267.01.03
Robinson, R., Kienast, M., Albuquerque, A., Altabet, M., Contreras, S., De Pol-Holz, R., Dubois, N., Francois, R., Galbraith, E., Hsu, T.-C., Ivanochko, T., Jaccard, S., Kao, S.-J., Kiefer, T., Kienast, S., Lehmann, M., Martinez, P., McCarthy, M., Moebius, J., Yang, J.-Y., 2012. A review of nitrogen isotopic alteration in marine sediments. Paleoceanography 27. https://doi.org/10.1029/2012PA002321
Ruan, J., Xu, Y., Ding, S., Wang, Y., Zhang, X., 2017. A biomarker record of temperature and phytoplankton community structure in the Okinawa Trough since the last glacial maximum. Quat. Res. 88, 89–97. https://doi.org/10.1017/qua.2017.28
Sanchez Goñi, M.F., Harrison, S.P., 2010. Millennial-scale climate variability and vegetation changes during the Last Glacial: Concepts and terminology. Quat. Sci. Rev. 29, 2823–2827. https://doi.org/10.1016/j.quascirev.2009.11.014
Sasaki, Y.N., Minobe, S., Asai, T., Inatsu, M., 2012. Influence of the Kuroshio in the East China Sea on the Early Summer (Baiu) Rain. J. Clim. 25, 6627–6645. https://doi.org/10.1175/JCLI-D-11-00727.1
Schubert, C.J., Calvert, S.E., 2001. Nitrogen and carbon isotopic composition of marine and terrestrial organic matter in Arctic Ocean sediments: implications for nutrient utilization and organic matter composition. Deep Sea Res. Part Oceanogr. Res. Pap. 48, 789–810. https://doi.org/10.1016/S0967-0637(00)00069-8
Shiozaki, T., Takeda, S., Itoh, S., Kodama, T., Liu, X., Hashihama, F., Furuya, K., 2015. Why is Trichodesmium abundant in the Kuroshio? Biogeosciences 12, 6931–6943. https://doi.org/10.5194/bg-12-6931-2015
Stein, R., 1991. Accumulation of Organic Carbon in Marine Sediments, Lecture Notes in Earth Sciences. Springer-Verlag, Berlin/Heidelberg. https://doi.org/10.1007/BFb0010382
Steinke, S., Hanebuth, T.J.J., Vogt, C., Stattegger, K., 2008. Sea level induced variations in clay mineral composition in the southwestern South China Sea over the past 17,000 yr. Mar. Geol. 250, 199–210. https://doi.org/10.1016/j.margeo.2008.01.005
Steinke, S., Mohtadi, M., Groeneveld, J., Lin, L.-C., Löwemark, L., Chen, M.-T., Rendle-Bühring, R., 2010. Reconstructing the southern South China Sea upper water column structure since the Last Glacial Maximum: Implications for the East Asian winter monsoon development. Paleoceanography 25, PA2219. https://doi.org/10.1029/2009PA001850
Sun, Y., Clemens, S.C., Morrill, C., Lin, X., Wang, X., An, Z., 2012. Influence of Atlantic meridional overturning circulation on the East Asian winter monsoon. Nat. Geosci. 5, 46–49. https://doi.org/10.1038/ngeo1326
Sun, Y., Oppo, D.W., Xiang, R., Liu, W., Gao, S., 2005. Last deglaciation in the Okinawa Trough: Subtropical northwest Pacific link to Northern Hemisphere and tropical climate. Paleoceanography 20. https://doi.org/10.1029/2004PA001061

Tian, Z., Jiang, D., 2020. Weakening and eastward shift of the tropical Pacific Walker circulation during the Last Glacial Maximum. Boreas 49, 200–210. https://doi.org/10.1111/bor.12417
Timmermann, A., Lorenz, S.J., An, S.I., Clement, A., Xie, S.P., 2007. The effect of orbital forcing on the mean climate and variability of the tropical Pacific. J. Clim. 20, 4147–4159.
Ujiié, H., Ujiié, Y., 1999. Late Quaternary course changes of the Kuroshio Current in the Ryukyu Arc region, northwestern Pacific Ocean. Mar. Micropaleontol. 37, 23–40. https://doi.org/10.1016/S0377-8398(99)00010-9
Ujiié, Y., Ujiié, H., Taira, A., Nakamura, T., Oguri, K., 2003. Spatial and temporal variability of surface water in the Kuroshio source region, Pacific Ocean, over the past 21,000 years: evidence from planktonic foraminifera. Mar. Micropaleontol. 49, 335–364. https://doi.org/10.1016/S0377-8398(03)00062-8
Verdel, C., van der Pluijm, B.A., Niemi, N., 2012. Variation of illite/muscovite 40Ar/39Ar age spectra during progressive low-grade metamorphism: an example from the US Cordillera. Contrib. Mineral. Petrol. 164, 521–536. https://doi.org/10.1007/s00410-012-0751-7
Vogt-Vincent, N.S., Mitarai, S., 2020. A Persistent Kuroshio in the Glacial East China Sea and Implications for Coral Paleobiogeography. Paleoceanogr. Paleoclimatology 35. https://doi.org/10.1029/2020PA003902
Wada, E., Hattori, A., 1976. Natural abundance of 15N in particulate organic matter in the North Pacific Ocean. Geochim. Cosmochim. Acta 40, 249–251. https://doi.org/10.1016/0016-7037(76)90183-6
Walker, M., Johnsen, S., Rasmussen, S.O., Popp, T., Steffensen, J.-P., Gibbard, P., Hoek, W., Lowe, J., Andrews, J., Björck, S., Cwynar, L.C., Hughen, K., Kershaw, P., Kromer, B., Litt, T., Lowe, D.J., Nakagawa, T., Newnham, R., Schwander, J., 2009. Formal definition and dating of the GSSP (Global Stratotype Section and Point) for the base of the Holocene using the Greenland NGRIP ice core, and selected auxiliary records. J. Quat. Sci. 24, 3–17. https://doi.org/10.1002/jqs.1227
Wan, S., Li, A., Clift, P.D., Stuut, J.-B.W., 2007. Development of the East Asian monsoon: Mineralogical and sedimentologic records in the northern South China Sea since 20 Ma. Palaeogeogr. Palaeoclimatol. Palaeoecol. 254, 561–582. https://doi.org/10.1016/j.palaeo.2007.07.009
Wan, S., Tian, J., Steinke, S., Li, A., Li, T., 2010. Evolution and variability of the East Asian summer monsoon during the Pliocene: Evidence from clay mineral records of the South China Sea. Palaeogeogr. Palaeoclimatol. Palaeoecol. 293, 237–247. https://doi.org/10.1016/j.palaeo.2010.05.025
Wan, S., Yu, Z., Clift, P.D., Sun, H., Li, A., Li, T., 2012. History of Asian eolian input to the West Philippine Sea over the last one million years. Palaeogeogr. Palaeoclimatol. Palaeoecol. 326–328, 152–159. https://doi.org/10.1016/j.palaeo.2012.02.015
Wang, J., Li, A., Xu, K., Zheng, X., Huang, J., 2015. Clay mineral and grain size studies of sediment provenances and paleoenvironment evolution in the middle Okinawa Trough since 17ka. Mar. Geol. 366, 49–61. https://doi.org/10.1016/j.margeo.2015.04.007
Wang, M., Liu, Z., Zhu, X., Yan, X., Zhang, Z., Zhao, R., 2019. Origin and formation of the Ryukyu Current revealed by HYCOM reanalysis. Acta Oceanol. Sin. 38, 1–10. https://doi.org/10.1007/s13131-018-1329-7
Wang, Q., Song, J., Yuan, H., Li, X., Li, N., Wang, Y., 2018. Sources and burial of particulate organic matter in the Kuroshio mainstream and its response to climate change over

the past millennium. Geo-Mar. Lett. 38, 497–511. https://doi.org/10.1007/s00367-018-0551-9

Wei, K.-Y., Mii, H.-S., Huang, C.-Y., 2005. Age Model and Oxygen Isotope Stratigraphy of Site ODP1202 in the Southern Okinaw a Trough, Northwestern Pacific. Terr. Atmospheric Ocean. Sci. 16, 001. https://doi.org/10.3319/TAO.2005.16.1.1(OT)

Wu, C., Fu, F.-X., Sun, J., Thangaraj, S., Pujari, L., 2018. Nitrogen Fixation by Trichodesmium and unicellular diazotrophs in the northern South China Sea and the Kuroshio in summer. Sci. Rep. 8, 2415. https://doi.org/10.1038/s41598-018-20743-0

Wu, C.-R., Chang, Y.-L., Oey, L.-Y., Chang, C.-W.J., Hsin, Y.-C., 2008. Air-sea interaction between tropical cyclone Nari and Kuroshio. Geophys. Res. Lett. 35. https://doi.org/10.1029/2008GL033942

Xu, K., Milliman, J.D., Yang, Z., Xu, H., 2007. Climatic and Anthropogenic Impacts on Water and Sediment Discharges from the Yangtze River (Changjiang), 1950–2005, in: Gupta, A. (Ed.), Large Rivers. John Wiley & Sons, Ltd, Chichester, UK, pp. 609–626. https://doi.org/10.1002/9780470723722.ch29

Xu, Z., Li, T., Clift, P.D., Lim, D., Wan, S., Chen, H., Tang, Z., Jiang, F., Xiong, Z., 2015. Quantitative estimates of Asian dust input to the western Philippine Sea in the mid-late Quaternary and its potential significance for paleoenvironment: ASIAN DUST INPUT TO WPS IN QUATERNARY. Geochem. Geophys. Geosystems 16, 3182–3196. https://doi.org/10.1002/2015GC005929

Xu, Z., Li, T., Clift, P.D., Wan, S., Lim, D., Chang, F., Sun, R., 2019. Sea-level, monsoonal, and anthropogenic impacts on the millennial-scale variability of siliciclastic sediment input into the western Philippine sea since 27 ka. J. Asian Earth Sci. 177, 250–262. https://doi.org/10.1016/j.jseaes.2019.04.001

Xu, Z., Wan, S., Colin, C., Li, T., Clift, P.D., Chang, F., Sun, R., Yu, Z., Lim, D., 2020. Enhanced terrigenous organic matter input and productivity on the western margin of the Western Pacific Warm Pool during the Quaternary sea-level lowstands: Forcing mechanisms and implications for the global carbon cycle. Quat. Sci. Rev. 232, 106211. https://doi.org/10.1016/j.quascirev.2020.106211

Yamamoto, M., 2009. Response of mid-latitude North Pacific surface temperatures to orbital forcing and linkage to the East Asian summer monsoon and tropical ocean-atmosphere interactions: response of North Pacific SST to orbital forcing. J. Quat. Sci. 24, 836–847. https://doi.org/10.1002/jqs.1255

Yanase, W., Abe-Ouchi, A., 2007. The LGM surface climate and atmospheric circulation over East Asia and the North Pacific in the PMIP2 coupled model simulations. Clim. Past 3, 439–451. https://doi.org/10.5194/cp-3-439-2007

Yang, Z., Li, T., Lei, Y., Chang, F., Nan, Q., 2020. Vegetation evolution-based hydrological climate history since LGM in southern South China Sea. Mar. Micropaleontol. 156, 101837. https://doi.org/10.1016/j.marmicro.2020.101837

Yu, S.-W., Tsai, L.L., Talling, P.J., Lin, A.T., Mii, H.-S., Chung, S.-H., Horng, C.-S., 2017. Sea level and climatic controls on turbidite occurrence for the past 26kyr on the flank of the Gaoping Canyon off SW Taiwan. Mar. Geol. 392, 140–150. https://doi.org/10.1016/j.margeo.2017.08.011

Yui, T.-F., Kao, S.-J., Wu, T.-W., 2009. Nitrogen and N-isotope variation during low-grade metamorphism of the Taiwan mountain belt. Geochem. J. 43, 15–27. https://doi.org/10.2343/geochemj.1.0003

Zhang, H., Liu, C., Jin, X., Shi, J., Zhao, S., Jian, Z., 2016. Dynamics of primary productivity in the northern South China Sea over the past 24,000 years: productivity in the South China Sea. Geochem. Geophys. Geosystems 17, 4878–4891. https://doi.org/10.1002/2016GC006602

Zhang, R., Chen, M., Cao, J., Ma, Q., Yang, J., Qiu, Y., 2012. Nitrogen fixation in the East China Sea and southern Yellow Sea during summer 2006. Mar. Ecol. Prog. Ser. 447, 77–86. https://doi.org/10.3354/meps09509

Zhao, D., Wan, S., Toucanne, S., Clift, P.D., Tada, R., Révillon, S., Kubota, Y., Zheng, X., Yu, Z., Huang, J., Jiang, H., Xu, Z., Shi, X., Li, A., 2017. Distinct control mechanism of fine-grained sediments from Yellow River and Kyushu supply in the northern Okinawa Trough since the last glacial. Geochem. Geophys. Geosystems 18, 2949–2969. https://doi.org/10.1002/2016GC006764

Zhao, Y., Liu, Z., Colin, C., Xie, X., Wu, Q., 2011. Turbidite deposition in the southern South China Sea during the last glacial: Evidence from grain-size and major elements records. Chin. Sci. Bull. 56, 3558–3565. https://doi.org/10.1007/s11434-011-4685-7

Zhao, Y., Zou, X., Liu, Q., Wang, C., Ge, C., Xu, M., 2018. Clay mineralogy indicates the muddy sediment provenance in the estuarine-inner shelf of the East China Sea. J. Asian Earth Sci. 152, 69–79. https://doi.org/10.1016/j.jseaes.2017.11.036

Zheng, L.-W., Hsiao, S.S.-Y., Ding, X.-D., Li, D., Chang, Y.-P., Kao, S.-J., 2015. Isotopic composition and speciation of sedimentary nitrogen and carbon in the Okinawa Trough over the past 30 ka. Paleoceanography 30, 1233–1244. https://doi.org/10.1002/2015PA002782

Zheng, X., Li, A., Kao, S., Gong, X., Frank, M., Kuhn, G., Cai, W., Yan, H., Wan, S., Zhang, H., Jiang, F., Hathorne, E., Chen, Z., Hu, B., 2016. Synchronicity of Kuroshio Current and climate system variability since the Last Glacial Maximum. Earth Planet. Sci. Lett. 452, 247–257. https://doi.org/10.1016/j.epsl.2016.07.028

Zhou, Y., Chen, F., Wu, C., Yu, S., Zhuang, C., 2016. Palaeoproductivity linked to monsoon variability in the northern slope of the South China Sea from the last 290 kyr: evidence of benthic foraminifera from Core SH7B. Geol. Soc. Lond. Spec. Publ. 429, 197–210. https://doi.org/10.1144/SP429.10

Ziegler, M., Jilbert, T., de Lange, G.J., Lourens, L.J., Reichart, G.-J., 2008. Bromine counts from XRF scanning as an estimate of the marine organic carbon content of sediment cores. Geochem. Geophys. Geosystems 9. https://doi.org/10.1029/2007GC001932

Zou, J., Chang, Y.-P., Zhu, A., Chen, M.-T., Kandasamy, S., Yang, H., Cui, J., Yu, P.-S., Shi, X., 2021. Sedimentary mercury and antimony revealed orbital-scale dynamics of the Kuroshio Current. Quat. Sci. Rev. 265, 107051. https://doi.org/10.1016/j.quascirev.2021.107051